

**Structural and dielectric studies of
magnesium substituted nano-crystalline
spinel zinc ferrites**



**By
Muhammad Zakir Hussain**

**School of Chemical and Materials Engineering (SCME)
National University of Sciences and Technology (NUST)
2018**

Structural and dielectric studies of magnesium substituted nano-crystalline spinel zinc ferrites



Muhammad Zakir Hussain

Regn. No. NUST201464632MSCME67914F

**This work is submitted as a dissertation in partial fulfillment of the
requirement for the degree of**

(MS in Nano Science & Engineering)

Supervisor Name: Dr. Khurram Yaqoob

**School of Chemical and Materials Engineering
National University of Sciences and Technology (NUST), H-12
Islamabad, Pakistan**

August, 2018

Dedication

I would like to dedicate this thesis to my beloved project Supervisor Dr. Khurram Yaqoob, Dr. I. H Gul, members of thermal transport lab, Lab Attendants, my family members (specially my mother) for their dedicated affection, and love leading me to success in life.

Acknowledgements:

All praise of almighty Allah, the most merciful and compassionate, the creator of the universe, who enabled me to complete this research work successfully. I feel privileged to have the honor to acknowledge my research supervisor Dr. Khurram Yaqoob and Dr. I. H. Gul to whom I owe my indescribable special indebtedness, who were very affectionate and cooperative during this research work. Without their kind and sincere efforts, it might have had not been possible for me to end this task in time. My Sincere regards to our Lab Attendants Mr. Zafar Iqbal, Mr. Khurram, Mr. Zeeshan and Mr. Shams who were always there to work with me all night long. Finally, I wish to offer my humble gratitude to my family especially my mother for their support in every sphere of my life that paved the way for me to reach this destination. I have realized that in my whole life, God blessed me just because of them.

Finally, the last but not the least, I'll say thanks to all, love and prayers I received from the above mentioned people, guiding me constantly in this world.

Sincerely

Muhammad Zakir Hussain

Abstract

In our reported study, Magnesium substituted Zinc ferrite nano-particles ($Zn_{1-x}Mg_xFe_2O_4$, where $x=0.0, 0.20, 0.35, 0.50, 0.65, 0.80, 1.0$) have been investigated. The samples were prepared via wet chemical co-precipitation route and were calcined at 800°C for six hours. Structural and dielectric properties of these samples were studied using XRD, SEM, FTIR and LCR meter. The XRD diffractograms confirmed the formation of FCC spinel structure with decreasing crystallite size from 19.2 nm to 34.2 nm without any additional impurity peak confirming the purity of the samples synthesized. The FTIR spectra confirmed the presence of tetrahedral (A) and octahedral (B) lattice sites in the structure confirming the spinel structure of synthesized nanoparticles. The SEM images confirmed the formation of nanoparticles. The agglomerates were also observed owing to the heat treatment (calcination) resulting in better diffusion of the atoms, causing the formation of agglomerates. No extra phase or impurity was found, confirming the effectiveness of co-precipitation route. The dielectric properties of the synthesized samples measured at room temperature against frequency range of 100 Hz to 5 MHz showed good enhancement of dielectric constant (on the order of 10^4 at 100 Hz) which was comparable to traditional ceramics (having dielectric constant in the range of 10^4 - 10^6), which are often rendered suitable for super capacitor applications. The dielectric loss Furthermore, the low values of dielectric loss tangent at high frequencies verified its potential usage in microwave applications. Significant contribution of both long and short range order in hopping as well as increase in grain boundary density was confirmed by complex electric modulus analysis.

Table of Contents

List of Figures.....	vii
List of Tables	viii
Abbreviations Page.....	ix
Chapter 1: Introduction.....	1
1.1 Spinel Ferrites:.....	1
1.2 Brief History	1
1.3 Source of Magnetism:.....	2
1.4 Classification of Magnetic Materials:	3
1.4.1 Diamagnetism:.....	3
1.4.2 Paramagnetism:	4
1.4.3 Ferrimagnetism & Ferromagnetism:	4
1.4.4 Anti-ferromagnetism:	4
1.4.5 Superparamagnetism:	5
1.5 Ferrites:.....	6
1.5.1 Soft Ferrites:	6
1.5.2 Hard Ferrites:.....	6
1.6 Types of Ferrites:.....	7
1.6.1 Spinal Ferrites:.....	7
1.6.1.1 Types of Spinel Ferrites:	8
1.6.2 Garnet Ferrites:	9
1.6.3 Hexagonal Ferrites:.....	9
1.7 Zinc Ferrites:	10
1.8 Advantage of ferrites over other Magnetic Materials:.....	11
1.9 Application of Ferrites:.....	12
1.10 Objectives:	15
Chapter 2: Literature Review	16
2.2. Literature survey.....	18
2.3 Chemical Co-Precipitation Method:.....	19
2.3.1 Major steps in Co-precipitation:	21
2.3.1.1 Co-precipitation:.....	21

2.3.1.2 Ferritization:	22
2.4. Parameters involved in Co-precipitation:	22
2.4.1 Temperature Effect:	22
2.4.2 Role of Anion:	22
2.4.3 Rate of mixing of the reactants:	22
2.4.4 Heating after Co-precipitation:	23
2.4.5 Effect of pH:	23
Chapter 3: Proposed Solution/Methodology:	24
3.1 Synthesis of ZnFe ₂ O ₄ :	24
3.1.1 Synthesis of Mg _{1-x} Zn _x Fe ₂ O ₄ (x=0.2, 0.35, 0.5, 0.65, 0.8, 1.0):	24
3.2 Introduction to Structural Characterization Techniques:	26
3.2.1 Introduction to X-Ray Diffraction:	26
3.2.1.1 Principle/Formulae of XRD:	27
Lattice constant	29
Crystallite Size	29
X-Ray Density:	29
Measured Density:	30
Porosity Fraction	30
3.2.2 Introduction to Scanning Electron Microscopy:	30
3.2.2.1 Principle of SEM:	30
3.2.3. Fourier Transmission Infrared Spectroscopy (FTIR)	31
3.2.4 Electrical Properties:	32
3.2.4.1 Dielectric Properties	32
Chapter 4: Results and Discussions:	34
4.1 X-ray Diffraction (XRD) Results:	34
Structure and morphology:	38
FTIR Spectra:	41
Dielectric Measurements:	42
Complex Electric Modulus:	48
Conclusion:	52
Future Work:	53

References 54

List of Figures

Figure 1: Spinel ferrite unit cell with octahedral and tetrahedral sites.....	8
Figure 2: Dipole orientation of dielectric	13
Figure 3: Chemical Co-precipitation steps	21
Figure 4: Scattering of incident X-ray Beam at plane of atoms in a crystal.....	27
Figure 5: Formation of a diffracted cone of radiations in powder method.....	28
Figure 6: Schematic diagram of Scanning Electron Microscope with CRT display.....	31
Figure 7- FTIR Spectrophotometer and basic principle	32
Figure 8: Indexed XRD pattern for $ZnFe_2O_4$	34
Figure 9: Indexed XRD pattern for $Mg_{0.2}Zn_{0.8}Fe_2O_4$	35
Figure 10: Indexed XRD pattern for $Mg_{0.35}Zn_{0.65}Fe_2O_4$	35
Figure 11: Indexed XRD pattern for $Mg_{0.5}Zn_{0.5}Fe_2O_4$	36
Figure 12: Indexed XRD pattern for $Mg_{0.65}Zn_{0.35}Fe_2O_4$	36
Figure 13: Indexed XRD pattern for $Mg_{0.8}Zn_{0.2}Fe_2O_4$	37
Figure 14: Indexed XRD pattern for $MgFe_2O_4$	37
Figure 15: SEM image of $ZnFe_2O_4$	39
Figure 16: SEM image of $Mg_{0.5}Zn_{0.5}Fe_2O_4$	40
Figure 17: SEM image of $MgFe_2O_4$	41
Figure 18: FTIR Spectra of synthesized ferrites.....	42
Figure 19: Dielectric Constant as a function of frequency.....	44
Figure 20: Dielectric Loss as a function of frequency.....	44
Figure 21: Tan Delta as a function of frequency	46
Figure 22: AC-Conductivity as a function of frequency	47
Figure 23: Variation of real (M') complex electric modulus as a function of frequency ...	48
Figure 24: Imaginary(M'') parts of complex electric modulus as a function of frequency	50
Figure 25: Cole Cole plot (M'' Vs M').....	51

List of Tables

Table 1. Materials classification based on magnetic susceptibility and some other properties	5
Table 2: Comparison between hard and soft ferrites	7
Table 3: Radii of some common metal ions used in the spinel ferrites.....	8
Table 4:Different types of ferrites	9
Table 5: Crystallite size (nm), Lattice constant (\AA), Volume of unit cell (\AA^3), Bulk density(g/cm^3), X-Ray density(g/cm^3) , Porosity fraction(P).....	39

Abbreviations Page

SEM	Scanning Electron Microscopy
FTIR	Fourier Transform Infrared
EMI	Electro-Magnetic Interference
XRD	X-Ray Diffraction
DC	Direct Current
AC	Alternating Current
HRTEM	High Resolution Transmission Electron Microscopy
FCC	Face Centered Cubic
FWHM	Full Width Half Maximum
CRT	Cathode Ray Tube
LCR	Inductance Capacitance Resistance Meter
SAED	Selected Area Electron Diffraction
VSM	Vibrating Sample Magnetometry

Chapter 1: Introduction

1.1 Spinel Ferrites:

In recent years spinel ferrites proved to be the most important nano sized, ferromagnetic ceramic materials which find numerous applications in electronic, magnetic and biomedical fields. Spinel ferrites are easy to synthesize, have low cost, high mechanical hardness, and high environmental stability. Sol-Gel, Co-precipitation and hydrothermal methods are the most common processes used for their synthesis. These methods may be classified into two categories namely, solid state methods and wet chemical methods. Among these two methods, wet chemical methods due to low sintering temperature required, small size and high homogeneity of particles obtained are usually preferred over solid state methods.

1.2 Brief History

The history of ferrites begins centuries before the birth of Christ, with the discovery of attraction property of stones. Most of these type of stones were found in Asia Minor in the Magnesia district (hence the derived term magnetism).

Chinese back in the 12th century used tiny magnets in compass and in various navigation applications. Later, navigators used ‘Lodestones’ to locate magnetic North was the first application of magnetite. During first scientific study of magnetism William Gilbert published De Magnete in 1600 A.D. He made some magnets artificially by rubbing iron with lodestones. In 1819 Hans C. Oersted observed compass needle shows a response near an electric current in a wire. After the great discovery of the fact that a magnetic field is produced by an electric current, the manufacturing of first electromagnet was done in 1825. Faraday, Bergmann and Becquerel later discussed the effect of magnetism on all the matter including liquids and gases. Further, with further contributions by Hertz, Maxwell, Faraday, and other scientists, developed the new science of electromagnetism.

The whole center revolves around the dipole and magnetic field perspectives to understand the concept of Magnetism. “Magnetic Field” in simple words, can be described as that space where there is an occurrence of energy change of the space. This variation in

energy can easily be measured and detected within the volume of space while the “Magnetic Poles” can be thought of the magnetic field detected to be entering or leaving the magnetic material. Magnetic poles can never be found existing in isolation, instead they occur forming a dipole, e.g. a bar magnet having two poles separated by a distance, a south (magnetic field is entering the dipole) and a north (magnetic field is leaving the dipole). Two dipoles or magnets can be created of a simple magnet bar is cut in half which can continue up to the atomic level. So the basic building block can be thought of as the source of magnetism. The property of a material, is called magnetism when the material will respond to the magnetic field. Some of the materials are attracted and some materials get repelled by the magnetic field and some are unaffected by the external magnetic field. Magnetic materials can be classified as under.

In magnetism two important quantities which relate M (magnetization) to H (magnetizing force) and B (magnetic flux density) to H (magnetizing force) i.e. magnetic permeability μ and magnetic susceptibility χ , which are defined as:

$$\mu = B/H \quad (1.1)$$

$$\chi = M/H \quad (1.2)$$

By nature, magnetite is a weak and ‘hard’ ferrite. Most ‘hard’ ferrites possess permanent magnetism. In 1930 J. L. Snoek become successful in producing a ‘soft’ ferrite at Phillips Research Laboratories in the Netherlands for commercial applications. Soft ferrite finds limited use that time and were originally synthesized in a selected sizes and shapes for antenna and inductor applications. Ferrites were predominately used in the areas of Electro-Magnetic Interference (EMI) suppression, power applications and low level applications.

1.3 Source of Magnetism:

Everything in the universe is made up of small building blocks called atoms, and in turn, these atoms are made up of neutrons, protons and electrons. Neutrons and protons are present inside nucleus of an atom, while electrons revolve around the nucleus in selected orbits. Magnetic field is produced by these revolving electrons as they move around the nucleus since they carry negative charge. The strength of this field is known as magnetic moment. On a subatomic scale it is quite difficult to imagine such a system. Let’s consider

an electronic current moving through a conductor. Magnetic field is created all around this conductor by the flowing of electrons. Such a field can be identified by movement of the compass needle. If we place a compass near the conductor, then a force will be experienced by the needle of compass showing magnetism. This is an example of dipole, because poles are being created on both sides of needle. Not only this, but every material responds uniquely around the magnetic field, in one way or the other.

1.4 Classification of Magnetic Materials:

Every material reacts differently upon its placement in the magnetic field of a magnet, because of the various factors such as molecular and atomic level of structure or the individual atoms magnetic moments. These moments are related with the electrons orbital and spin motion in an atom, both these motions are affected by the applied external magnetic field. Some materials magnetic moments get aligned parallel to the applied field while others get are aligned opposite to the applied field. On the other hand, insulators show no response to the applied magnetic field [1].

In atoms, electrons are usually present in pairs in their orbitals, due to their opposite spins they cancel out each other's magnet field. Materials with unpaired electrons possess some net magnetic field. Based upon the different characteristics, material's magnetic behavior can be classified as:

1. Paramagnetism
2. Diamagnetism
3. Ferro/Ferrimagnetism
4. Anti-ferromagnetism
5. Superparamagnetism

1.4.1 Diamagnetism:

Diamagnetism of a material is referred to be a result of electrons orbital motion in an external applied magnetic field. The direction of electrons alignment is opposite to the direction of applied field thus resulting in repulsion of material in opposite direction. Diamagnetism occurs due to zero net magnetic moment of an electron. The field direction created by orbital motion is opposite in direction to the external applied field which is

represented by a negative susceptibility, as illustrated in Fig.1. These type of materials tend to move toward weaker field regions.

1.4.2 Paramagnetism:

Paramagnetism behavior is the incomplete or partial cancellation of spin/orbital electron magnetic moments resulting in a permanent dipole moment [2]. There is no net magnetization on domain size in absence of magnetic field i.e. the dipoles in the domains are oriented randomly. Their moments aligned themselves by rotation upon the application of the magnetic field, towards the field direction, thus acquiring a net magnetization.

1.4.3 Ferrimagnetism & Ferromagnetism:

Ferri and ferro-magnetic materials, possess a very large permanent magnetization and in the absence of an applied field a permanent magnetic moment. In ferro type materials, there are atomic domains in which large number of atomic spins align themselves in the direction of external field, creating permanent magnetic moment.

On the other hand, in ferrimagnetic materials lower permanent magnetization results from the magnetic dipoles incomplete cancellation in a domain (Fig 1). Macroscopically magnetization of ferri- and ferro-magnetic materials is equal to the sum of the domain magnetizations in the sample [3]. Most ferromagnets are metals (conductors) whereas ferrimagnets are ionic solids i.e. to some extent these are electrical insulators.

1.4.4 Anti-ferromagnetism:

In anti-ferromagnetic behavior, the magnetic moments associated with the atoms or molecule, related to the electron spin, are usually aligned in a regular pattern with the neighboring spin oriented oppositely. Usually such a behavior exists at very low temperatures, diminishing at and above a specific temperature which is known as Neel Temperature [4].

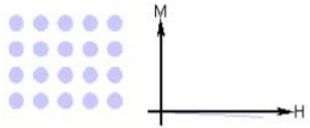
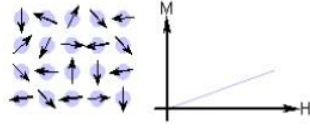
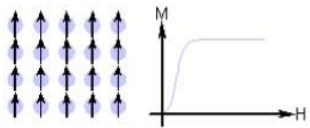
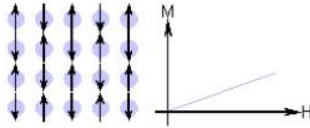
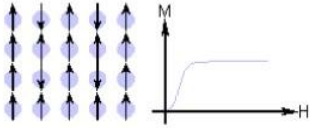
Type of magnetism	Magnetic susceptibility, χ	Atomic / Magnetic Behavior	Temperature dependence	Examples and comments
Diamagnetic	Negative and small, Au: -2.74×10^{-6} Cu: -0.77×10^{-6}		Temperature independent	The shells of the atoms are closed as in the case of covalent solids such as Ge, Si, and metals such as Au, Cu, Ag, etc.
Paramagnetic	Positive and small, β -Sn: 0.19×10^{-6} Pt: 21.04×10^{-6} Mn: 66.10×10^{-6} 10^{-5} - 10^{-4}		Temperature independent	Atoms have randomly oriented magnetic moments as in alkali and transition metals
	Positive and small		Follows Curie or Curie-Weiss law: $\chi = \frac{C}{T - \theta}$	Atoms constituting the material have a permanent magnetic moment as in ferromagnets (Fe), antiferromagnets (Cr), ferrimagnets (Fe_2O_3) at high temperatures
Ferromagnetic	Positive and large, function of applied field, microstructure dependent Fe: $\sim 100,000$		Ferromagnetic below Curie temperature and paramagnetic above it	Atoms have parallel aligned magnetic moments, possesses large permanent magnetization even without external magnetic field as in some transition metals and rare earths such as Fe, Co, Ni, Gd, Dy
Antiferromagnetic	Positive and small, Cr: 3.6×10^{-6}		Antiferromagnetic below the Néel temperature and paramagnetic above it	Atoms have mixed parallel and anti-parallel aligned magnetic moments. Primarily oxides and salts of transition metals such as MnO, NiO, MnF_2 .
Ferrimagnetic	Positive and large, function of applied field, microstructure dependent, Ba ferrite: ~ 3		Ferrimagnetic below the Curie temperature and paramagnetic above it	Atoms have anti-parallel aligned magnetic moments, possesses large magnetization even without external magnetic field

Table 1. Materials classification based on magnetic susceptibility and some other properties

1.4.5 Superparamagnetism:

In sufficiently small material particles, under the influence of temperature magnetization randomly flip direction. Similar to a paramagnet, an external field magnetize the particles, in this state. Their magnetic susceptibility of these materials is much larger than that of paramagnets. The phenomenon where a material exhibits magnetic behavior similar to that of paramagnetism when heated below curie temperature or Néel temperature is called superparamagnetism. Normally, due to magnetic materials coupling forces cause magnetic moment alignment of neighboring atoms, this results in enhancement of internal magnetic fields [5].

1.5 Ferrites:

Ferrites are the most important ferrimagnetic materials. Iron oxide (Fe_2O_3) is the principal component in the ferrites. Due to presence of ferrimagnetic oxides ferrites are insulating materials. Ferrites are generally magnetic materials that are used to make cores of transformer, permanent magnets and in other so many applications. These are mostly used in the high frequency application as they restrict the production of eddy currents because of high resistivity. The value of electrical resistivity of ferrites is very high [1]. Depending upon the charge and mass of metal ions, there are two structural symmetries of ferrites. One is the cubical other is hexagonal structure. There are two types of ferrites based on the hysteresis losses.

1.5.1 Soft Ferrites:

Soft ferrites are generally known by the lower coercivity values. The materials which have the low value of energy dissipation in magnetization or demagnetization have low value of coercivity [1]. They appear dark black or gray. These are very hard and brittle. Soft ferrites have high value of resistivity. These are used to prevent the energy losses like in inductors and the cores of transformers. Some examples of soft ferrites are Mn-Zn ferrite and Ni-Zn ferrite.

1.5.2 Hard Ferrites:

These are generally known as ceramic magnets. Hard ferrites have the high value of coercivity. High coercivity means the material take large time to demagnetize. The magnetic permeability of the hard ferrites is very high. Hard ferrites are made of iron, strontium and barium oxides. Hard ferrites are very cheap in cost. As the raw material is easily available to make hard ferrites. These are being used excessively in the house hold things due to their low cost. Some of the important hard ferrites are ferrite, strontium ferrite and cobalt ferrite [1]. Comparison between the two types of ferrites has been shown in the table given below.

Table 2: Comparison between hard and soft ferrites

Soft magnetic	Hard magnetic	Hard magnetic	Hard magnetic
Low Coercivity (Hc)		High Coercivity (Hc)	
Low Saturation Magnetization		High saturation magnetization	
Low Permeability		High Permeability	
Low Remanence		High Remanence	
Low Magnetostriction		High Magnetostriction	
Low Curie temperature (Tc)		High Curie temperature (Tc)	

1.6 Types of Ferrites:

There are three types of ferrites depending upon the structure of ferrites. Which can be categorized as under.

1.6.1 Spinal Ferrites:

These ferrites have general formula of MFe_2O_4 . Here M is a divalent cation. Mg^{+2} , Ni^{+2} , Co^{+2} , Zn^{+2} and Cu^{+2} are the examples of divalent cations. Compared to its other ferrite types spinal ferrites have the simpler structure. Spinel lattice is composed of 32 Oxygen ions in a unit cell. In a face centered cubic structure (fcc) the anions are arranged in a close-packing. The space sites between the anions are two types, we refer as A and B sites.

(A). Tetrahedral sites

(B). Octahedral sites

In a spinel structure there are a total of 64 tetrahedral sites. Out of 64, cations occupy 8 of the tetrahedral sites. On the other hand, 6 oxygen atoms surround the octahedral site. There are a total of 32 octahedral sites in the spinal ferrite structure. 16 octahedral sites are occupied by anions. The complete occupation of the A and B sites result into an electrically neutral structure of spinal ferrite. Some common metal ions radii used in the spinel ferrites [1] are shown in Table 3.

Table 3: Radii of some common metal ions used in the spinel ferrites

Ion	Ionic radius Å
Fe ²⁺	0.83
Fe ³⁺	0.67
Co ²⁺	0.82
Zn ²⁺	0.74
Ni ²⁺	0.78
Mn ³⁺	0.70

1.6.1.1 Types of Spinel Ferrites:

There are two types of spinel structure:

- (a) Normal spinel
- (b) Inverse spinel

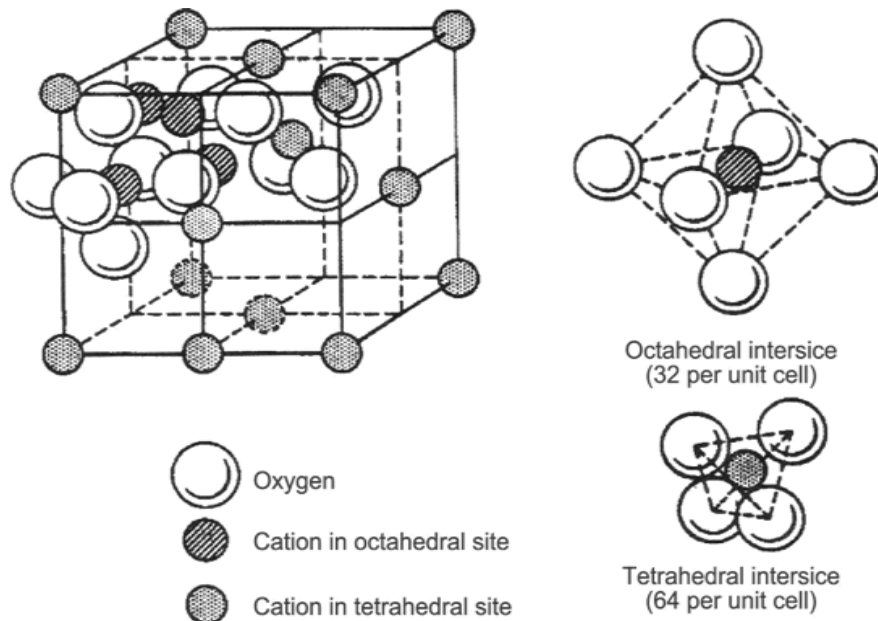


Figure 1: Spinel ferrite unit cell with octahedral and tetrahedral sites

(Adopted from: Materials Science and Engineering: An Introduction,
7th Edition, Chapter 20: Magnetic Properties)

In normal spinel ferrites, all trivalent metal ions are present at the B sites and divalent metal ions occupy A-sites in crystal structure. Whereas, in inverse spinel structure B-sites are occupied by all divalent metal ions in the crystal structure, also trivalent ions occupy both these A and B sites [1].

1.6.2 Garnet Ferrites:

Garnet ferrites have cubic structure with the general formula $M_3Fe_5O_{12}$. Where M is the rare earth metal trivalent ion. The Garnet ferrites were first discovered in 1957 by Gilleo and Giller. Rare earth metal ions of Y, Gd, and Dy are the examples of the trivalent metal ions. These ferrites are magnetically hard materials.

1.6.3 Hexagonal Ferrites:

Hexagonal ferrites are generally represented by the formula $MFe_{12}O_{19}$. Here M can be barium, cobalt, strontium or the combination of these. Hexagonal ferrites are generally used as permanent magnet because of its high value of coercivity [1]. Spinal and hexagonal structures are almost similar to each other with little difference. In hexagonal structures metal ions are located in the structure at three different sites i.e. at octahedral, tetrahedral and trigonal sites. These hexagonal structured magnetic materials are commonly used as magnetic recording devices, in loud speakers, in microwave applications, as fridge magnets and also widely used in every field. Below table shows some examples of the different crystal structures of ferrites and the elements commonly used in these structures:

Table 4: Different types of ferrites

Type	Structure	General Formula	Example
Spinel	Cubic	$M^{II}Fe_2O_4$	M^{II} =Fe, Cd, Co, Mg, Ni and Zn
Garnet	Cubic	$M^{III}_3Fe_2O_{12}$	M^{III} =Y, Sm, Eu, Gd, Tb, and Lu
Magnetoplumbite	Hexagonal	$M^{II}Fe_{12}O_{19}$	M^{II} =Ba, Sr

1.7 Zinc Ferrites:

Zinc ferrite is a very important material. Zinc ferrite appears to be a tan colored solid material which is insoluble in water, in dilute alkali and acids. It has captured the attention of the researchers due to so many useful applications in magnetic fluids, magnetic recording devices, high resistivity and many more. Zinc ferrite (ZnFe_2O_4) has good chemical stability and excellent mechanical hardness. Zinc ferrites are the cubic ferrites. These have the spinel structure where Fe^{+3} ion is located at octahedral sites and Zn^{+2} is located at tetrahedral sites. For the synthesis of zinc ferrite nanoparticles co-precipitation and sol-gel processes are widely used. Commonly used salts contain Fe (III) and Fe (II) for the synthesis of the zinc ferrite nanoparticles. Because of their high opacity, zinc ferrites find its use as pigments, where heat stability is required e.g., zinc ferrite synthesized from iron oxide can be used at temperatures above 177°C . Zinc ferrite is also used as effective anti-corrosion element when it is added to corrosion-resistant coatings, it is seen that the anti-corrosion property of materials increases with increase in zinc ferrite concentration. Zinc ferrite in the bulk form is generally paramagnetic, but when it is converted into thin film form it becomes ferrimagnetic. By controlling thin films growth conditions of zinc ferrite high room temperature magnetization have been achieved. The electrical, dielectric properties of the zinc ferrite are of great concern. There are so many applications related to the electrical and dielectric properties of the ferrites. A lot of work has been done on these properties. Dielectric constant, dielectric loss, ac and dc electrical resistivity and conductivity are very dependent on the crystal structure, grain size of the zinc ferrite. On the other hand, grain size and crystal structure are dependent on the method of synthesis by which the material is formed.

AC conductivity (σ_{ac}) of ferrite increase by increasing the frequency. The dielectric loss in the crystal lattice is due to the impurities and imperfection. Increase in the frequency also increases the dielectric constant (ϵ'). Up to 10 kHz the dielectric constant increases. The dielectric constant decreases on further increase in frequency. The reason for this change in dielectric constant with the frequency is that the ferrites conversion from ferromagnetic to paramagnetic on changing the frequencies. With change in the temperature dielectric constant (ϵ') also changes.

Magnesium:

Magnesium, Mg-24 having atomic weight of 24.305 amu and atomic number of 12 is a shiny gray solid. It is an important member of group 2 of periodic table along with other 5 elements of group 2 family. Group 2 of periodic is generally known as alkaline earth metals group. According to its abundance it is amongst 9 of the most abundant elements found in the universe and 8th amongst most abundant elements found on earth's crust and in the earth it is 4th most common element. It is also dissolved seawater where it is 3rd most abundant element after sodium and chlorine.

Naturally Mg occurs in combination with other elements, found in oxidation states of +2 and +1. It has an atomic radius of 160 pm. Mg has electrical resistivity and magnetic susceptibility of 43.9 nΩ.m and $+13.1 \cdot 10^{-6} \text{ cm}^3/\text{mol}$ respectively at room temperature. It is paramagnetic in nature. Its density is less than Al, so when used in making alloys it gives lightness and strength to the material. It is also important element in our body as it is basic unit of cells and numerous enzymes. Magnesium ions are essential for the smooth functioning of enzymes in our body. It is also the third most important structural material after iron and aluminum.

Mg has excellent electrical properties, low weight and good mechanical strength that makes it widespread use in the manufacturing of electronic devices such as mobile phones, laptops, cameras and also other electronic components. Magnesium is also used for charge storage in batteries. In the oxide form magnesium, due to its high thermal and electrical resistance properties, it is used in fire-resistant cables as an electrical insulator. In the printing industry it is used in photoengraving plates as an alloy with zinc. As Al-Mg alloy it is used in sports items, in aircraft and automobile engine parts and bodies.

1.8 Advantage of ferrites over other Magnetic Materials:

Iron (Fe) and other metallic alloys having low DC resistivity make them technologically useful magnetic materials. However, these are not suitable to use for high frequency applications such as inductor core circuits. The problem of such low resistivity is that excessive heat is generated in response of the induced currents in these materials. This becomes a serious problem because useful energy is wasted and released in the atmosphere. So as the frequency gets higher, the loss useful energy makes such materials inefficient and less effective. On the other hand, seeing at the high DC electrical resistivity and thermal

stability of ferrites, these can be as a potential candidate for good electrical performance. Ferrites are capable of good electrical performance at higher frequency ranges with its additional capability of wide range temperature stability and high permeability. These characteristics have expanded the use of ferrites in wide band and high frequency transformers, high frequency electronic circuitry, inductors delay lines, quality filter circuits and others. They are generally economical than other magnetic alloys and metals. For the optimum combination of high stability, high inductor quality, low cost and low volume to work in the range from 10kHz to a few hundred MHz ferrites are the best core material of choice. Furthermore, ferrites possess unique magnetic and mechanical parameters that are flexible that none other material have.

1.9 Application of Ferrites:

In the nanometer scale ferrite particles of any type and combination are very important magnetic materials as they have wide applications in technology, because of their high electric resistivity, particularly at high frequencies [6]. Due to their following properties ferrite nano-particles are used widely

- ✓ Wide selection of materials
- ✓ Usefulness at microwave frequencies
- ✓ Mechanical stiffness
- ✓ Cheap
- ✓ High frequency applications
- ✓ High Coercivity
- ✓ High temperature stability

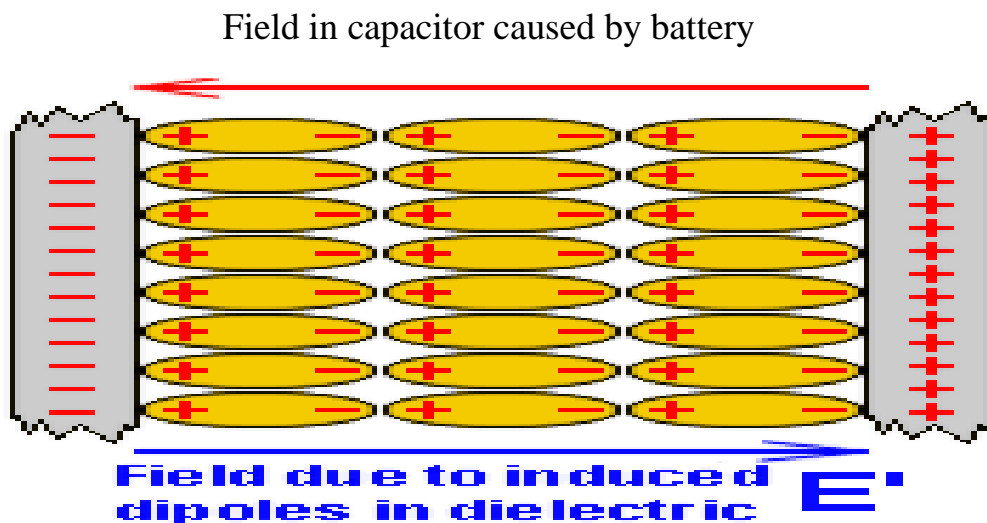
Due to their high ($>10^6 \Omega\text{-cm}$) DC electrical resistivity ferrite nano-materials are chosen. Moreover, their good magnetic properties, chemical stability over wide temperature range and low eddy current losses, they have potential applications in:

- ✓ Data storage
- ✓ Drug delivery
- ✓ Electromagnetic absorbers
- ✓ Microwave devices
- ✓ Ferro-fluids

✓ Core of Materials

Among the ferrites, those having general formula of MFe_2O_4 (where $M = Zn, Fe, Cu, Ni, Co, Mg$ etc.) zinc ferrite is a spinal soft magnetic material having significant electrical, magnetic and optical properties. Zinc ferrite also have good chemical stability, corrosion resistance and reasonable cost. It can be synthesized by using different chemical routes including, co-precipitation, solvo-thermal, hydrothermal, sol-gel, and micro-emulsion etc. Considering the properties of metals like Mg, Cu and Ag as well as zinc ferrite, coupling of these metals with zinc ferrite would have wide range of additional potential applications from electromagnetic devices to biomedics, can be utilized for drug delivery, water purification, magnetic data storage, and magnetic force microscopy etc [7].

With the burning of fossil fuel climate changes are increasing. Despite the advantages because of its versatile form, huge disadvantage of electricity is also incorporated with it. Its storage is relatively difficult to, for example, to store large amount of charge/electric power, batteries require hours and hours of continuous charging. Capacitors on the other hand, require little time to get charged but it has the disadvantage to store only little amount of charge. To overcome these limitations, we need to synthesize such materials that can store and release huge amount of charge/electricity at the same time. An enhancement of dielectric properties of material is one way to overcome this.



Field due to induced dipoles in dielectric

Figure 2: Dipole orientation of dielectric

(Source: Wikipedia, "Working of Capacitors")

Let's suppose two electrically neutral, conducting metal plates and are separated by a distance 'd'. If these plates are connected to the battery in such a way that the positive terminal (anode) of battery is connected to one plate and negative terminal (cathode) of battery is connected to other plate, then a potential is created between these two plates. At this stage, although there is no charge flowing between the plates, because there is physical contact between the positive and negative terminal of battery, but a net potential is created between the plates. After the removal of battery, the charge will be stored momentarily on the plates, these charges have the ability to do useful electric work. plates If we place an insulating or non-conducting material between these plates, separated by a distance d, then this material is called a dielectric material. There are two functions of this material, one is to keep the charges at a distance d, so as to create a potential between the plates and secondly doing the useful electric work by allowing the electric field that is generated by the potential between the plates to align the dipoles along the lines of electric field, this gives more and more charge storage ability to the capacitor as shown in Figure 2. Mathematically, capacitance is represented by,

$$C = \epsilon_0 A / d$$

Capacitance 'C' has direct relation with area 'A' of parallel plates and an inverse relation with thickness 'd' dielectric material. So, in order to further enhance the capability of the capacitor, we have to either decrease the thickness of material between the plates or increase the area of plates. Increase in area is makes a limitation of space and decrease in thickness of dielectric material can lead to the limitation of charge storage. So to overcome this shortcoming, our present study is focused on doping of different combination of metal (i.e. Mg) and zinc ferrite and study their behavior and effect on the dielectric property of composite material formed.

For the synthesis of different combinations of zinc ferrite nanoparticles co-precipitation (wet chemical route), was employed. Different combinations of zinc ferrite nanoparticles i.e. $ZnFe_2O_4$, $Mg_{0.2}Zn_{0.8}Fe_2O_4$, $Mg_{0.35}Zn_{0.65}Fe_2O_4$ $Mg_{0.5}Zn_{0.5}Fe_2O_4$ were prepared. The prepared composites where completely homogenized by applying solid state method. XRD technique confirmed the spinel structure of the ferrite and material microstructure was confirmed by Scanning Electron Microscopy (SEM). Composites were analyzed by using Agilent E4991A material analyzer.

1.10 Objectives:

The present work is carried out with following objectives

- Synthesis of single phase spinel ferrite nanoparticles of ZnFe_2O_4 using an inexpensive and simple chemical co-precipitation
- To synthesize ZnFe_2O_4 composites (i.e. $\text{Mg}_x\text{Zn}_{1-x}\text{Fe}_2\text{O}_4$, where $x=0.2, 0.35, 0.5, 0.65, 0.80, 1.0$) by co-precipitation method
- To study and compare the dielectric properties of the synthesized nanoparticles.

Chapter 2: Literature Review

The literature survey on the subject is carried out systematically. Since long time, different compositions of spinel ferrites have been studied and also these are used in many practical applications. A vast research has been done on spinel ferrites, it is very difficult to collect all the information and experimental results about the work done so far in every aspect. The given literature review is only restricted to the systematic review of different theoretical and experimental facts related to present study including Zn and Mg based Spinel ferrites.

Nanoparticles can be synthesized by any of the following approaches namely

- Top down approach
- Bottom up approach

Top down:

In this approach large scale or bulk material is cut and divided into nano scale material. Etching lithography and mechanical attrition are examples of such approach e.g. grinding of bulk metal into nanoscale powder by ball milling.

Bottom up:

In this approach, nanoparticles are synthesized by combination of small building blocks i.e. atoms, molecules and clusters. Nanoparticles prepared by aerosols compaction and chemical synthesis are examples of this approach synthesis [8]. Nanoparticles are synthesized by different methods. Each method has its own merits and demerits. Magnetic, electrical and structural properties change as our method of synthesis change. Some of the methods used for nanoparticles synthesis are listed below:

- ✓ Co-precipitation method
- ✓ Sol-Gel Method
- ✓ Combustion Flame Synthesis
- ✓ PolyVinyl Alcohol Evaporation Technique
- ✓ Gas Condensation Process
- ✓ Microemulsion Method
- ✓ Sono-Chmeical Method

Chemical Co-precipitation method for the nanoparticles synthesis was used in this research work. The details of this method are discussed here.

Nanoparticles of ZnFe_2O_4 have been synthesized via Co-precipitation (chemical route). XRD studies confirms single phase, face centered cubic spinel structure of nanoparticles. XRD data also provides the crystallite size of the nanoparticles synthesized. ZnFe_2O_4 and all its different combinations of composite nano-crystalline single phases (i.e. $\text{Mg}_{0.2}\text{Zn}_{0.8}\text{Fe}_2\text{O}_4$, $\text{Mg}_{0.35}\text{Zn}_{0.65}\text{Fe}_2\text{O}_4$ $\text{Mg}_{0.5}\text{Zn}_{0.5}\text{Fe}_2\text{O}_4$) were prepared and calcined at $800\text{ }^\circ\text{C}$ for 6 hours by following the chemical route. The influence of Mg^{+2} on properties of Zn-ferrite was investigated. The temperature effect on calcination was investigated by means of XRD and Scanning Electron Microscopy (SEM). Due to unlimited fossil fuel consumption, and considering the fact that environmental degradation and energy crisis is rapidly increasing, i.e. to explore those resources that are sustainable and ecosystem friendly [9-10]. Innovations in storage systems with prolonged service life time, environmental integrity, maintaining high power density meanwhile having the quality to quickly charged/discharged have forced the researchers to progress in the field of high charge storage capacity super-capacitors [10-12]. In recent years the trend of combination of two or more materials with different dielectric properties enhanced the dielectric properties of each constituent and the composite material. Zinc ferrite is a spinel magnetic nano-material, among other ferrites with the general formula MFe_2O_4 (where $\text{M} = \text{Zn, Fe, Co, Ni, Mn, etc}$), having low coercivity, high resistivity significant optical, magnetic and electrical properties [7]. Material scientists are giving increased attention nano structured zinc ferrite due to its unique properties. Zinc ferrite has been used for the purification of coal gas from NO , H_2S and CO_2 like toxic gases and as an adsorbent material for de-sulfurization of hot-gas. Photocatalytic properties of ZnFe_2O_4 has also been reported. Fe^{+3} ions occupy all the octahedral sites and Zn^{+2} ions occupy all the tetrahedral sites in bulk form at room temperature. But going to nano-level scale and below Neel's temperature the magnetic behavior of ZnFe_2O_4 is transformed from paramagnetic to ferrimagnetic and weak anti-ferromagnetic. This happens when ferrite and metal cations exchange their position between the octahedral sites and tetrahedral sites. Thus inversion of cations in the sites and particle size variation change the properties exhibited by ZnFe_2O_4 . Nanoparticles of ZnFe_2O_4 synthesized by ball milling, combustion synthesis, sol-gel and co-precipitation exhibit

ferrimagnetic behavior. In the present work ZnFe_2O_4 were synthesized by using co-precipitation route. Its structural, dielectric properties and electrical conductivity after doping with different combination of Mg were studied. For nano-ferrites preparation co-precipitation method is reliable, cost-effective, simple and low temperature method. In present work the dielectric loss (ϵ''), dielectric constant (ϵ'), AC conductivity, $\tan(\delta)$ and structural behavior of ZnFe_2O_4 and its different composites with Mg (i.e. $\text{Mg}_x\text{Zn}_{1-x}\text{Fe}_2\text{O}_4$, where $x=0.2, 0.35, 0.5, 0.65, 0.80, 1.0$) as function of variable frequency were studied.

2.2. Literature survey

In 2018 Pankaj Choudhary and Dinesh Varshney synthesized Cu^{+2} substituted Mg-Zn nanoferrite ($\text{Mg}_{0.5}\text{Zn}_{0.5-x}\text{Cu}_x\text{Fe}_2\text{O}_4$) by sol-gel auto combustion method. XRD confirmed their spinel nature. The crystallite size of synthesized particles was in the range 22.25–29.19 nm. There is an increase in ac conductivity of nanoferrites with increase in the frequency. Presence of dielectric relaxation in nanoferrites is showed. At 1 Mhz, and $x=0.2$, ohmic nature was observed by a large semicircle. A minimum loss of 0.009, high dielectric constant and high ac conductivity value was seen at 1 Mhz frequency.

In 2015 T.A. Elmosalami, S.H. Al-Heniti, H.M. Zaki, using co-precipitation method synthesized $\text{Mg}_{0.5}\text{Zn}_{0.5-x}\text{Cu}_x\text{Fe}_2\text{O}_4$ ($x = 0.0, 0.1, 0.2, 0.3, 0.4$ and 0.5) nano-crystalline ferrite. Magnetic and structural properties were investigated with influence of Cu^{+2} ions. XRD revealed single cubic spinel phase of ferrite in nano-crystalline form. With increase in the concentration of Cu^{+2} lattice constant 'a' decreased. Initially up to $x=0.2$ there is an increase in saturation magnetization on further increase of Cu^{+2} ions it showed a decreasing trend. AC conductivity, dielectric constant ϵ' , dielectric loss ϵ'' , loss tangent and $\tan\delta$ as a function of temperature and frequency were calculated. Cu^{+2} substitution influence on AC conductivity is seen at low 'f' and low temperatures ≤ 100 °C. Dielectric loss ϵ'' and constant ϵ' showed an increasing trend with increase in temperature.

In 2009 Zeljka Cveji, Srdan Rakic, Stevan Jankov, Sonja Skuban, Agne Kapo showed the role of grain size, chemical composition and method of synthesis on electrical properties of spinel ferrites. Co-precipitation method was used by them to synthesize the nanosized $\text{Y}_{0.15}\text{Zn}_{0.85}\text{Fe}_2\text{O}_4$ and ZnFe_2O_4 and powders. The AC conductivity, dielectric constant, loss factor in the frequency range 1Hz to 100kHz and in temperature range 300 to 350K was

investigated. Koops model was used for the explanation of the different trends of dielectric permittivity (ϵ) and electrical conductivity with increasing frequency. In frequency range 1 to 10kHz $\tan\delta$ show maximum value.

In 2018 Sven Warfsmann, Dereje Hailu Taffa, Michael Wark used electrochemical method to synthesize zinc ferrite films. The deposited films were converted to crystalline nature from amorphous nature by heat treatment at 600 °C. TEM and XRD were used for their morphological and structural characterization. Photo electrochemical measurements show n-type semiconductor nature of films. The ratio of Zn:Fe decides the magnitude of the photocurrent at the surface.

In 2014 A.G. Mostafa, R.M. Megahid, Ashraf S. Elkady, Shaban I. Hussein, M.M. Rashad, synthesized MgFe_2O_4 from EDTA/sol-gel method. MgFe_2O_4 powders were calcined at different temperatures of 600°C, 500°C and 400°C. HRTEM, XRD, FTIR, and VSM were applied for magnetic and structural properties of particles. Depending upon calcination temperature, cubic and tetragonal phases of spinel MgFe_2O_4 were revealed by XRD. Size of nano-crystallite varied from 8.933 to 41.583 nm, and depending on calcination temperature cubic and tetragonal phases size vary from 1.379 to 292.565 nm respectively. In the cubic phase the Mg^{+2} ions occupy B-sites and Fe^{+3} ions occupy octahedral B-sites and tetrahedral A-sites equally and show mixed spinel structure. While in tetragonal phase it is an inverse spinel. The crystalline spinel structure was confirmed by SAED and HRTEM. VSM showed fractional superparamagnetic nature of particles at room temperature while at 400 °C pure superparamagnetic behavior observed. It is showed that magnetic properties of Mg-ferrite changed with the change of calcination temperature.

2.3 Chemical Co-Precipitation Method:

Generally co-precipitation method is used to synthesize electro ceramics nanopowders, that are formed in a very short time in complex oxides form. However, emission of fumes accompanied with technique is a disadvantage of this method. Nucleation, growth, coarsening and/or agglomeration processes for the formation of nanoparticles simultaneously occur in a co-precipitation reaction. When product precipitation begins, initially small crystallites form (nucleation), but these are converted to larger form as they aggregate together quickly to form more electrostatically stable particles (growth). During the growth process the smaller particles are utilized by larger particles (coarsening). A

relatively slow growth process and relatively fast nucleation process is what that is required to produce nano-particles. The absence of subsequent nucleation of smaller particles and simultaneous formation of all the nuclei of species present is essential for the narrow size distribution of the particles formed.

There are generally two categories of reaction for synthesis of oxides, one of that produces a precursor which must be further subjected to treatment like drying and calcination and in the other one gives oxide directly. The metal hydroxides obtained from the first process are usually are in form of precipitates (either containing chlorides or nitrates) in H_2O on addition of basic solution such as NaOH or $NH_4(OH)$. The resulting chlorides or nitrates are washed away and the residue is calcined after washing, drying and grinding to obtain the oxide powder. Co-precipitation method is a very wonderful method to create the fine particles of nano size [13]. The ferrites obtained by this method are homogeneous and pure in their chemistry and composition that is way co-precipitation procedure is very fine method to obtain ferrites. By the control of pH by adding NaOH the various salts like sulphates, nitrates and chlorides results into the oxide nanoparticles in a co-precipitation process. In co-precipitation process the particle size is also dependent on the pH of the starting precursors. On the other hand, molarity of the chemicals defines the particle size of the material.

The chemical transport of ions and chemical rate of reaction is affected by the concentration of the chemicals. The crystallinity of the particles is affected by the reaction rate and the impurities present in the solution. Growth rate, nucleation and super saturation affects the particle shape and size to some extent. At high super saturation the size of particle becomes small. As precipitating agent, usually NaOH is preferred [14]. For the precipitation of particles to occur, reasonable temperature and optimum pH value is required for the purpose. The whole process of co-precipitation can be shown as block diagram (Fig 3)

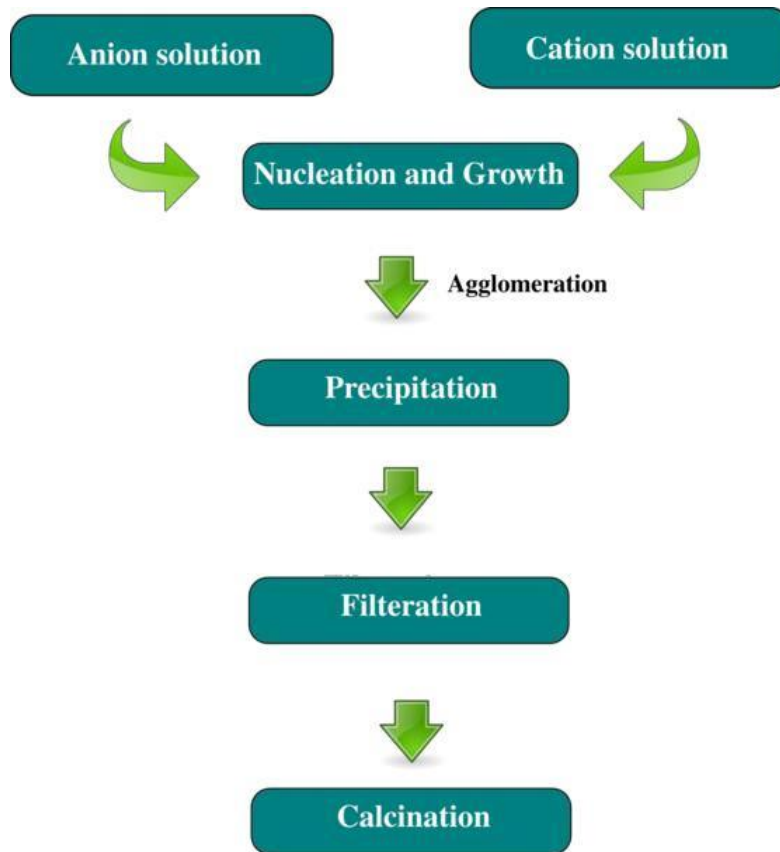


Figure 3: **Chemical Co-precipitation steps**

(Source: **Nucleation Processes in Catalysis, Volume 2**)

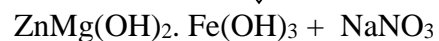
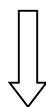
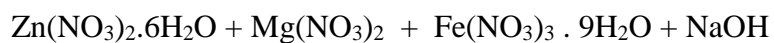
2.3.1 Major steps in Co-precipitation:

Co-precipitation involves two major steps that are

- Co-precipitation
- Ferritization

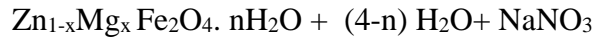
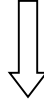
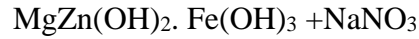
2.3.1.1 Co-precipitation:

In this step, we obtain colloidal particles of metal hydroxides that are synthesized by the co-precipitation of dissolved metal cations in an alkaline medium. For Mg-Zn ferrites the reaction is:



2.3.1.2 Ferritization:

The product obtained in the first step is transformed to MgZn-ferrites from metal hydroxides solution by heating the precipitated alkaline solution,



In co-precipitation, the precipitate formation, the size and shape of the particles formed during the process is influenced by temperature, quantity of chemicals added etc. Washing of the product with deionized water several times until the pH reaches to neutral removes the ionic impurities like Na and NO₃.

2.4. Parameters involved in Co-precipitation:

Some parameters and their influence on the co-precipitation process can be described as

2.4.1 Temperature Effect:

Different metals have the different values of activation energy for the ferrites formation. The activation energy is obtained from the heat given to the reactants. For the formation of cobalt ferrites use mostly use the reaction temperature in the range 70-100 centigrade.

2.4.2 Role of Anion:

The properties of the particles formed in the co-precipitation process is also dependent on the types of anions used. Anions may be in the form of metal ion solutions or in the form of salts. For good results the use of the metal salts is recommended. The metal salts can be the sulphates, nitrates or chlorides.

2.4.3 Rate of mixing of the reactants:

The size of the particles is greatly influenced by the rate of mixing of reactants. In the co-precipitation process growth and nucleation are the two important processes. When the nucleation rate is higher than the growth rate and the growth rate is slow, then small size particles are formed. In the same way when nucleation rate is low as compared to the growth rate then large particles are formed. Mixing of the precursors rate in the first case is very high and rate of mixing is low in the second case [15]. Particles of homogeneous chemistry

is obtained by slow mixing.

2.4.4 Heating after Co-precipitation:

When the co-precipitation process is completed for the formation of the required phase annealing is required. The level and duration of heating is impotent in the sense of the required size and shape of the particles depends on these factors.

2.4.5 Effect of pH:

PH plays an important role in the synthesis of controlled size and shape particles. At low values of pH the growth of the particles is no significant. On increasing the value of the pH the growth rate of the particle yield is high enough. Increase in the pH value decreases the time required for the synthesis of the product. In our case of zinc ferrite composites the pH range is 13-14 which is decreased by washing till 7.

Chemical co-precipitation process has many advantages over other synthesis techniques.

- Particle composition is controllable
- Rapid and simple preparation of particles
- Mono-dispersed and homogeneous particles formation
- Particle shape and size are easily controllable

Chapter 3: Proposed Solution/Methodology:

3.1 Synthesis of ZnFe₂O₄:

For the preparation of nominal composition ZnFe₂O₄, the chemicals used for Co-precipitation were Fe(NO₃)₂.9H₂O (iron nitrate) and Zn(NO₃)₂.6H₂O (zinc nitrate) with NaOH to control the PH to about 13-14 for the co precipitation of metal hydroxide to occur, which is then subsequently neutralized by washing the sample with de-ionized water. The respective composition was made using the simple stoichiometric formula:

$$\text{Mass} = \frac{\text{Molarity} \times \text{Molecular Mass} \times 100}{1000}$$

0.1 Molar (100ml) Solution of Zn(NO₃)₂.6H₂O (Zinc Nitrate (II) Hexahydrate) and 0.2 Molar (100ml) solution of Fe(NO₃)₃.9H₂O (Iron Nitrate(III) Nonahydrate) were prepared by using deionized and distilled water that were combined with each other by stirring on a hot plate at the room temperature for about 10 min. With constant stirring mixture was heated to 80 °C a 2 Molar (100ml) soln. of NaOH that was simultaneously heated to 80 °C was added dropwise to the solution. The temperature of solution was constantly maintained at 80 °C to with constant stirring for 45 min. The product was eventually cooled down followed by washing several times with double distilled deionized water for removal of the impurities from zinc ferrite particles that is present in the solution as a precipitate. The precipitate was dried in the oven at 100 °C overnight and then grinded in piston and mortar. The powder obtained after drying and grinding of sample was further calcined in a Muffle Furnace at 800 °C for 6 hours to obtain distinct phase of nanoparticles after the removal of carbonaceous impurities. The resultant powder was grinded using Mortar and Pestle to eliminate agglomeration and the powder was characterized using XRD, FTIR, and SEM.

In terms of calculating dielectric properties, hydraulic press was used to compress the powder into pellets. The load applied was 4tons and the pallets were obtained in round cylindrical form. Palette was sintered for about 2 to 3 hours in a simple furnace at 550 °C.

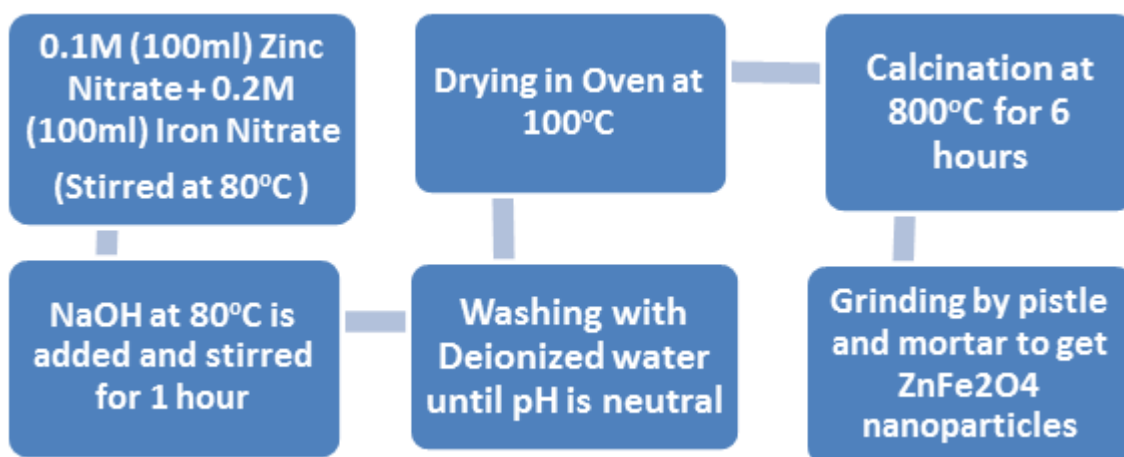
3.1.1 Synthesis of Mg_{1-x}Zn_xFe₂O₄ (x=0.2, 0.35, 0.5, 0.65, 0.8, 1.0):

Magnesium substituted zinc ferrites (i.e. Mg_{1-x}Zn_xFe₂O₄, where x = 0.2, 0.35, 0.5, 0.65, 0.8, 1.0) samples were synthesized by the co-precipitation method. Aqueous solutions of iron

nitrate nonahydrate, magnesium nitrate hexahydrate and zinc nitrate hexhydrate in the molar ratio (Fe:Mg:Zn=2:0:1, 2:0.2:0.8, 2:0.35:0.65, 2:0.5:0.5, 2:0.65:0.35, 2:0.80:0.20 and 2:1:0) with the required stoichiometric amount were prepared separately. All the three solutions were then mixed in a one beaker and heated slowly up to 80 °C with constant stirring. 2 molar solution of sodium hydroxide was prepared in a separate beaker and was heated to 80 °C with constant stirring. With constant stirring mixture was heated to 80 °C a 2 Molar (100ml) soln. of NaOH that was simultaneously heated to 80 °C was added dropwise to the solution. The solution temperature was constantly maintained at 80 °C for 45 min with constant stirring. The product was eventually cooled down followed by washing several times with distilled and deionized water for removal of the impurities from magnesium zinc ferrite particles that are present in the solution as a precipitate. The precipitate was dried in the oven at 100 °C overnight and then grinded in piston and mortar. The powder obtained after drying and grinding of sample was further calcined in a Muffle Furnace at 800 °C for 6 hours to obtain distinct phase of nanoparticles after the removal of carbonaceous impurities. The resultant powder was grinded in Mortar and Pestle to eliminate agglomeration and the powder was characterized using XRD, FTIR, and SEM.

In terms of calculating dielectric properties, hydraulic press was used to compress the powder into pellets. The load applied was 4 tons and the pallets were obtained in round cylindrical form. Palette was sintered for about 2 to 3 hours in a simple furnace at 550 °C.

The overall procedure for the experimentation is shown below.



3.2 Introduction to Structural Characterization Techniques:

To analyze the effect of Mg on Zn-ferrite nano composites following tests were performed.

X-Ray Diffraction

- Porosity Calculations
- Lattice parameter determination
- Particle Size
- Phase formation confirmation
- Bulk/Mass Density
- X-ray Density calculations

Scanning Electron Microscopy

- Morphology
- Structural observations

Electrical Studies

- Dielectric Measurements

FTIR spectroscopy

- Study of functional groups

3.2.1 Introduction to X-Ray Diffraction:

The principle of XRD lies in the fact that X-ray wavelength is comparable to the narrow interatomic distances between atoms of the material. XRD serves as a major and most useful characterization tool for the study of structure and degree of crystallinity of crystals. It not only provides us with the information like crystallite size, crystal defects, structural strains and degree of crystallinity but also the information of phase and crystal orientation. Powder diffraction, Laue's and rotating crystal methods are the three different approaches for the determination of crystal structure. The size of crystal is determined by powder method by two techniques.

- Diffractometer method
- Debye Sherrer Method

Cu and Mo like source materials are often used for sample analysis in an XRD. Cu- $k\alpha=1.54$ as a source is used in our analysis.

3.2.1.1 Principle/Formulae of XRD:

The beam of X-Ray striking the crystal structure is just like the beam is striking consecutive mirrors i.e. the angle of incident x-ray beam striking different planes of crystal is equal to angle of reflection of beam from the crystal structure. After reflection from different planes the x-ray undergoes constructive interference from each set of crystal planes. According to Bragg's Law,

$$n\lambda=2d\sin\theta\text{..... (3.1)}$$

where n =interference order, d =interlayer distance, θ =angle of incidence and λ =Wavelength of incident X-rays

Braggs law states, when equally spaced planes separated by distance d is incident upon by a ray in such a way that the reflected wave makes an angle θ with the normal then their path difference is given by $2d\sin\theta$ [16]. For constructive interference to happen the following condition must be followed,

$$2d\sin\theta = n\lambda$$

where $n=1,2,3\text{.....}$

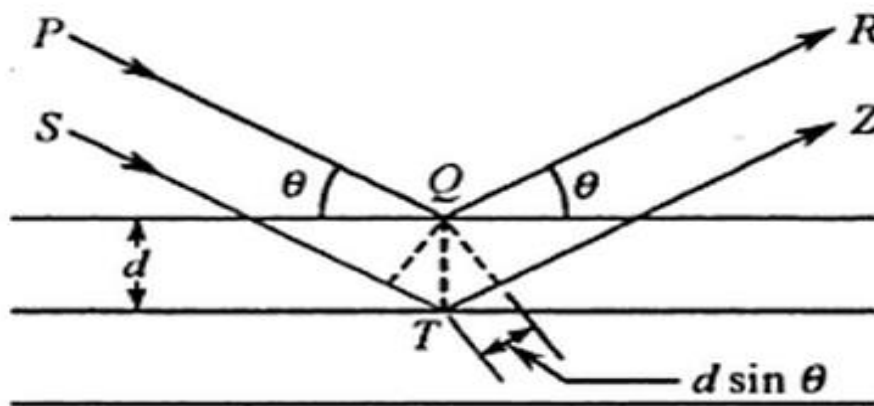


Figure 4: Scattering of incident X-ray Beam at plane of atoms in a crystal

The above equation is known as Bragg's Equation. Reflection can only occur when wavelength of incident beam is less than twice the distance between the planes i.e. $\lambda < 2d$. For this reason, x-rays are preferred over visible light in XRD.

To obtain 3D structures in XRD the following techniques are commonly used,

- (i) Rotating Crystal Method
- (i) Powder method
- (ii) Laue Method

We use the powder method for the analysis of our powdered material as our sample is also in the nano powdered form. Powdered samples are best evaluated with powder diffraction method when single crystals of acceptable size are not available. This method gives the suitable choice to find crystal structure and gives best results in powder form samples and there is no need of making single crystals. In this work, the sample in the form of very fine ground powder was placed in an Al or glass made rectangular shaped plate, where it is incident upon by a monochromatic X-ray beam,

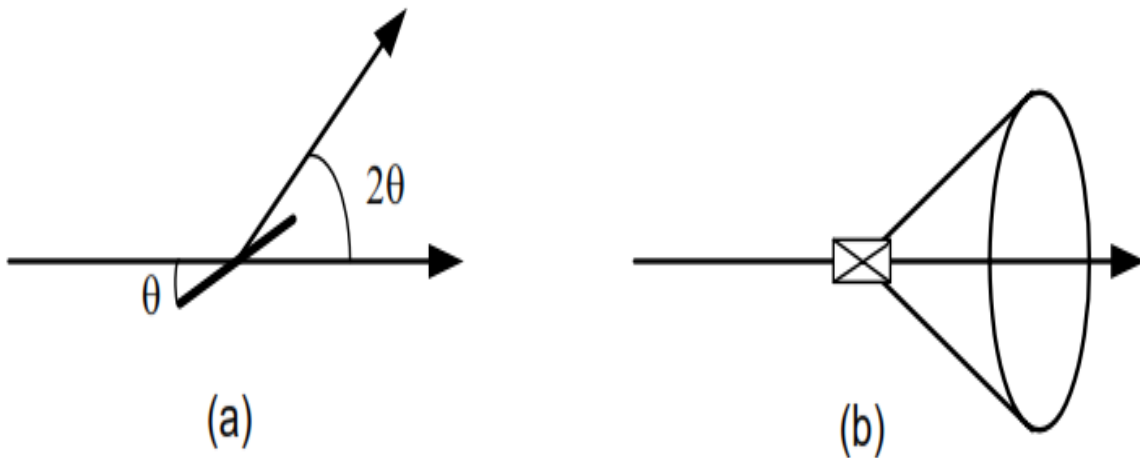


Figure 5: **Formation of a diffracted cone of radiations in powder method.**

Consider reflection of incident beam as shown in Fig. 4 and Fig. 5. When the x-ray beam is directed on the surface of fraction of powdered crystals this beam will be reflected back from (h,k,l) planes of the crystal obeying Bragg's law. Keeping constant angle theta when the plane is rotated along the incident beam, a cone of reflected beam is formed. Crystal particles will give equivalent reflection as some of them will fulfil Braggs law. By knowing the angle of reflection θ and wavelength λ of incident beam, inter planner spacing d can be calculated.

Lattice constant

Lattice constant or lattice parameter 'a' is defined as the angle between unit cell edges or the length of one of the edge of unit cell of crystal lattice. Lattice constant defines the constant distance between the points of crystal lattice. To calculate the lattice constant following equation is used,

$$a = \lambda (h^2 + k^2 + l^2)^{1/2} / 2 \sin \theta \dots\dots\dots(3.2)$$

Where a is the lattice parameter/constant, (h, k and l) are the miller indices, λ is the wavelength of X-ray radiation (1.54 for Cu- α) and θ is the diffraction angle,.

Crystallite Size

For phase identification and confirmation JCPDS cards are used for the verification comparison of experimentally obtained diffraction patterns. Structural properties are greatly influenced by the size of particles. Peak width in an XRD spectrum is inversely proportional to the particle size of the material. Small crystallite size in an XRD corresponds to the peak broadening in the spectrum. Debye Sherrer equation is used to estimate the crystallite size of particle. Particle size is calculated using the above mentioned equation. By using FWHM (Full-Width-Half-Maximum) value of pattern peaks subsequent index and putting it in the Sherrer equation one can estimate the crystal size of material,

$$t = \frac{0.9\lambda}{\beta \cos \theta} \dots\dots\dots 3.3$$

Where β is FWHM value of respective peaks, λ is the wavelength of the incident X-ray and θ is the diffraction angle.

X-Ray Density:

XRD data can be used to calculate the X-ray density of crystal material. By knowing the lattice constant 'a' of each individual sample we can calculate the x-ray density by using the equation,

$$\rho_x = ZM/Na^3 \dots\dots (3.4)$$

where a=lattice constant, M=Molecular weight of sample, Z=8 as the structure is cubic and contains 8 atoms per cell and N=Avogadro's Number (6.03×10^{23})

Measured Density:

Bulk density and measured density are related to the materials intrinsic property. It is calculated by using the conventional formula of density,

$$\rho_m = m/\pi r^2 h \dots (3.5)$$

Here m=mass, r=radius, h=thickness of the sample pellet. For pellet formation hydraulic press and sample die is used to convert the sample into a pellet. Density calculation of sample is done by knowing the mass and volume of this pellet. The radius and thickness of pellet are measured by Vernier caliper and mass of pellet is measured using analytical balance. By putting the value of mass and thickness of pellet resultant density is calculated [17].

Porosity Fraction

The general trend of increase or decrease in porosity with change in compositions of material is shown by porosity fraction,

$$\text{Porosity Fraction} = I - pm/px \dots (3.6)$$

3.2.2 Introduction to Scanning Electron Microscopy:

Scanning Electron Microscopy (SEM) utilizes a high energy beam of electrons to image the sample surface. It is an electron imaging technique which provides image of sample morphology as well as the bulk material. This high energy incident electron beam interacts the surface of sample and provides us with useful information of sample such as,

- Composition of the sample
- Sample surface topography
- Phase mapping
- Morphology

By the interaction of beam with the sample surface various types of signals are generated which may include characteristic x-rays, back scattered electrons, secondary electrons, cathodoluminescence and transmitted electrons.

3.2.2.1 Principle of SEM:

In SEM, the high energy beam of electrons is incident upon surface of sample using raster scan in a very narrow cross sectional area. The incident electrons interaction with surface

results in the emission of photons and electrons from the surface. A combination of different set of solid state detectors are used to collect these electrons and photons. The cathode ray tube brightness is controlled by the output of these detectors. An image on the Cathode Ray Tube display is shown by electron beam rastering X and Y voltages in accordance with the X and Y inputs; CRT displays every point impinged by the beam. Backscattered and secondary electron images, and elemental X-ray maps are the three types of images produced by SEM [18].

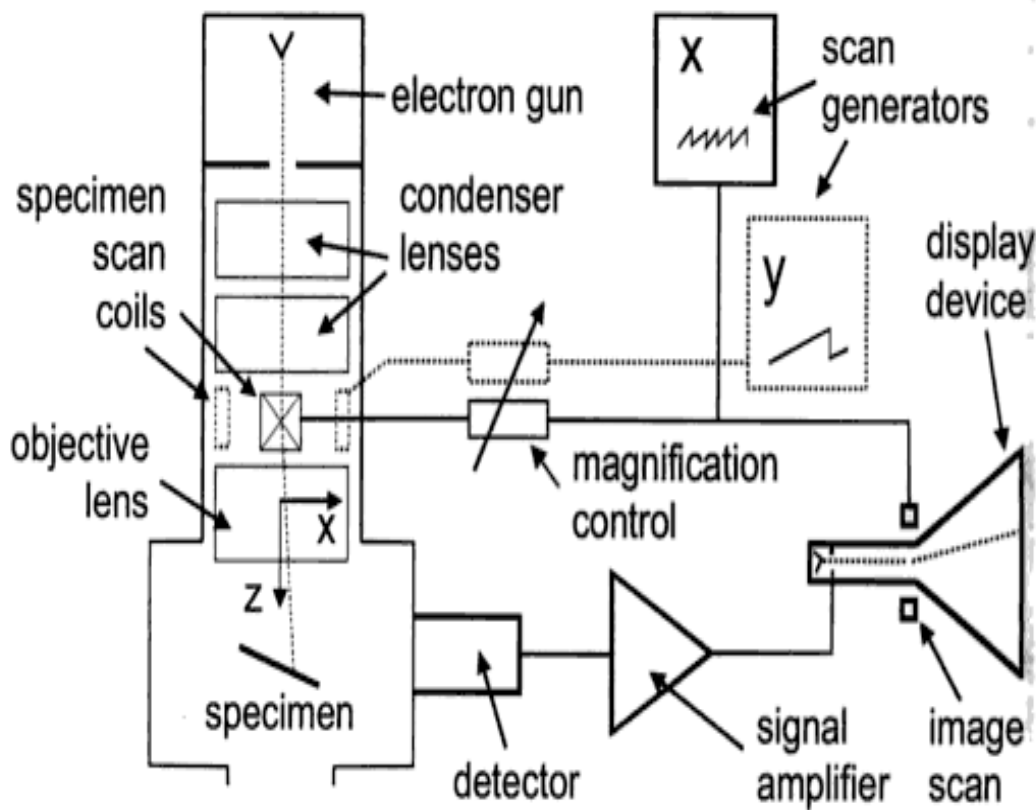


Figure 6: Schematic diagram of Scanning Electron Microscope with CRT display

3.2.3. Fourier Transmission Infrared Spectroscopy (FTIR)

In the field of polymers, analytical chemistry, industrial research and food industry FTIR is the most versatile technique. It also finds its use in detection of functional groups and to determine mechanism of chemical. IR region (12800 to 10 cm^{-1}) can be divided into three further regions i.e. near IR ($4000\sim 12800\text{ cm}^{-1}$) mid IR ($200\sim 4000\text{ cm}^{-1}$) and far IR ($50\sim 1000\text{ cm}^{-1}$). To determine the functional groups in structure elucidation this technique is mainly

used. For solid powder, samples are analysed for functional group identification mostly by making KBr pellets by using hydraulic press and sample die.

IR range of (350~4000) is used for most inorganic ions and organic compounds.

The sample were run on FTIR as shown in figure 7.

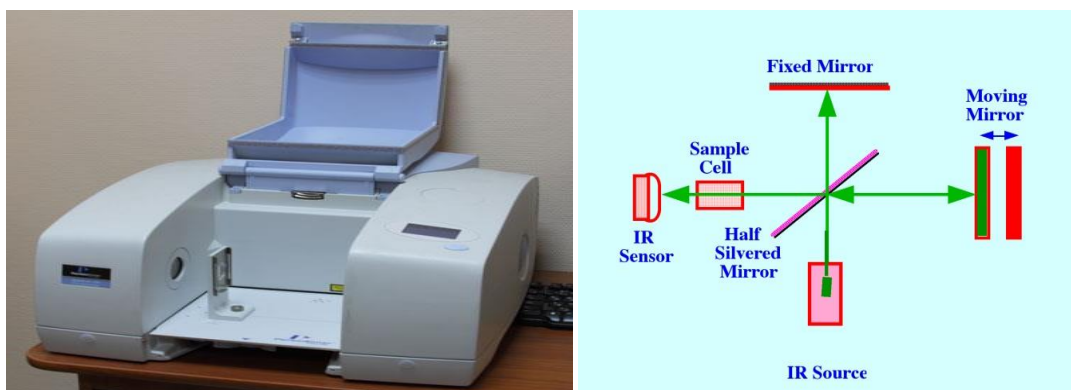


Figure 7- FTIR Spectrophotometer and basic principle

3.2.4 Electrical Properties:

3.2.4.1 Dielectric Properties

LCR meter bridge is used to measure the dielectric constant and dielectric loss factor of the sample pellet. After formation of sample pellet capacitance was measured directly from the LCR meter and then by using the formula dielectric constant was calculated

$$\epsilon' = Cd / (A \epsilon^0) \quad (3.9)$$

where d is thickness of pellet in meters, C is the capacitance in farad, ϵ_0 is permittivity of free space and is equal to 8.85×10^{-12} F/m and A is the cross-sectional area of surface of the pellet. The relation to calculate dielectric loss (ϵ'') from dielectric constant (ϵ') is given by,

$$\epsilon'' = \epsilon' \times D$$

where D is the energy dissipation factor.

During the rotation of dipole, the dipole encounters frictional damping force within the material. To overcome, the dipole has to do work against the damping force. In doing so it loses some power to overcome the frictional force [26-28]. $\tan \delta$ (dielectric loss tangent) can be determined in terms of real (ϵ') and imaginary (ϵ'') parts of dielectric constant, i.e.

$$\tan \delta = D = \epsilon'' / \epsilon' \dots\dots\dots(3.10)$$

AC-Conductivity, resulting because of the hopping mechanism is calculated using the equation

$$\sigma_{AC} = \omega \epsilon^0 \epsilon' \tan \delta \dots\dots\dots(3.11)$$

Chapter 4: Results and Discussions:

4.1 X-ray Diffraction (XRD) Results:

The Powder X-Ray Diffraction Technique was employed to investigate the phase and structure formation of the prepared Zinc-ferrite composites

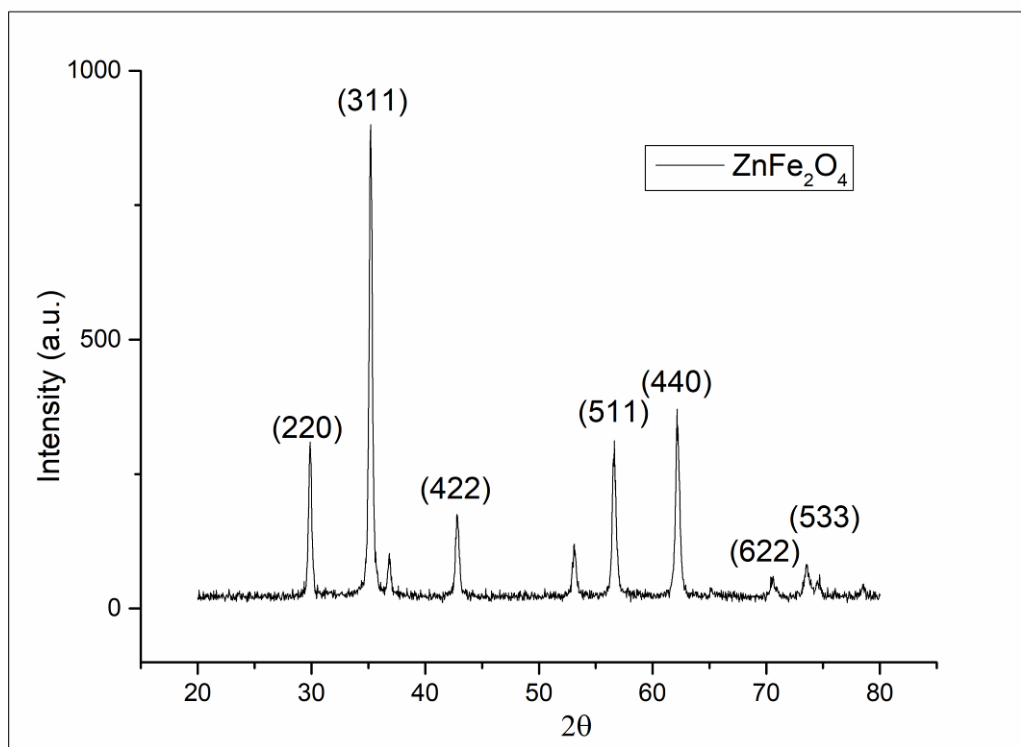


Figure 8: Indexed XRD pattern for ZnFe₂O₄

ZnFe₂O₄ nanoparticles closed packed FCC structure was confirmed by XRD of the pure ferrite powder (Fig 8-14). Samples were calcined at 800°C for 6 hours. The ZnFe₂O₄ nanoparticles structure is found in accordance with JCPD card number # 01-089-1012. The distinct appearance of the peak (311) at 35.2712° shows crystallinity of the synthesized product while the FWHM shows the formation of a small crystallite size which in turn confirms the formation of small grain size. No additional peak appeared (other than that of cubic arrangement) on the pattern which means that no impurity was present in the synthesized product. The crystallite size was calculated to be 34.2 nm using the Debye Scherer formula.

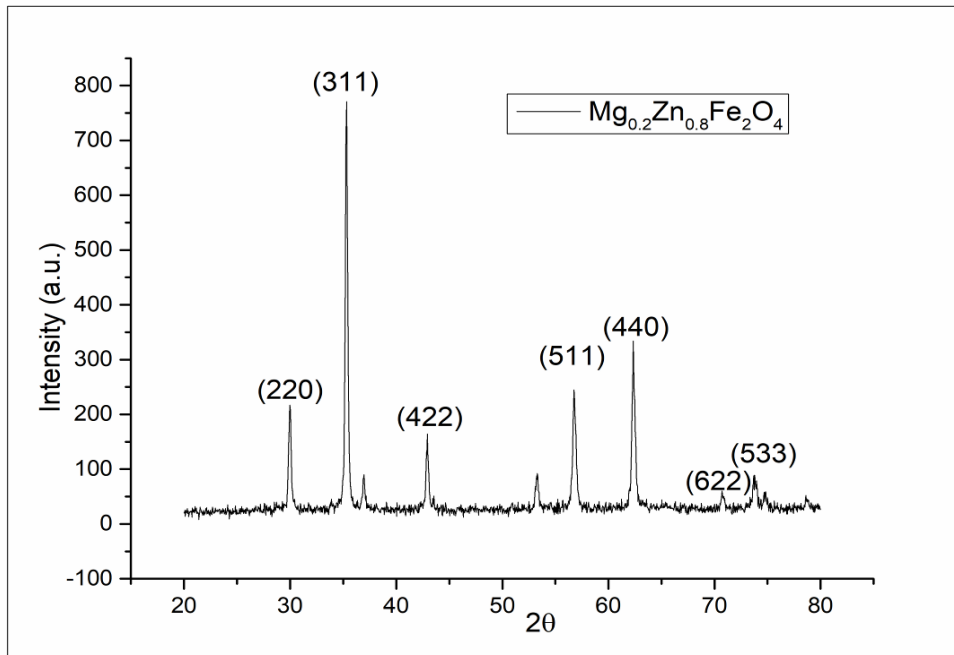


Figure 9: Indexed XRD pattern for $\text{Mg}_{0.2}\text{Zn}_{0.8}\text{Fe}_2\text{O}_4$

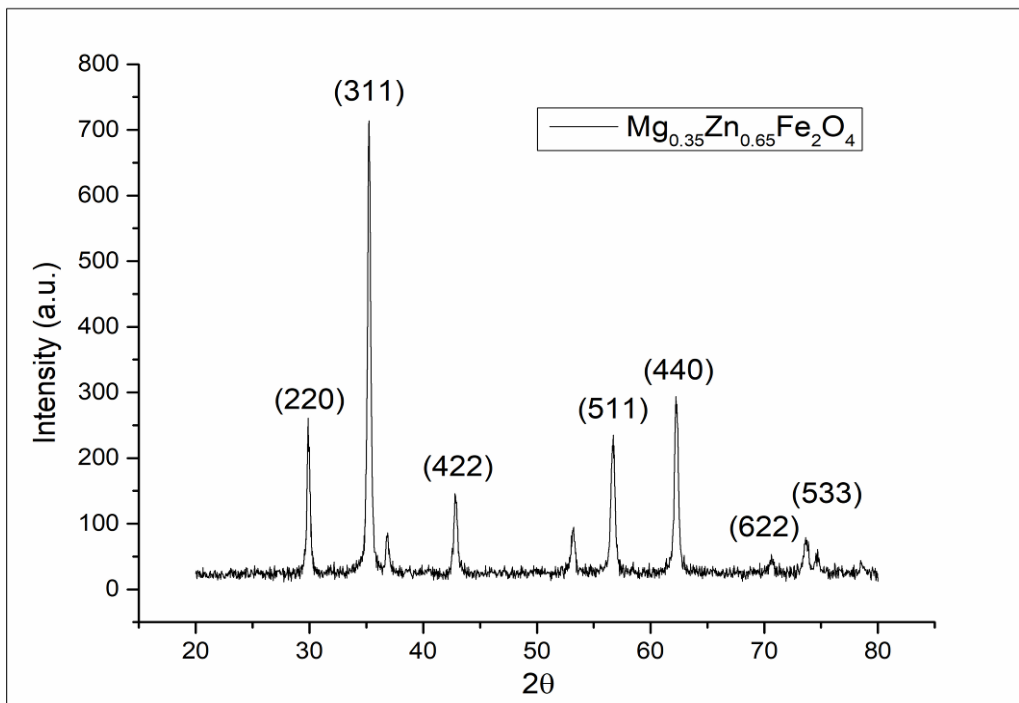


Figure 10: Indexed XRD pattern for $\text{Mg}_{0.35}\text{Zn}_{0.65}\text{Fe}_2\text{O}_4$

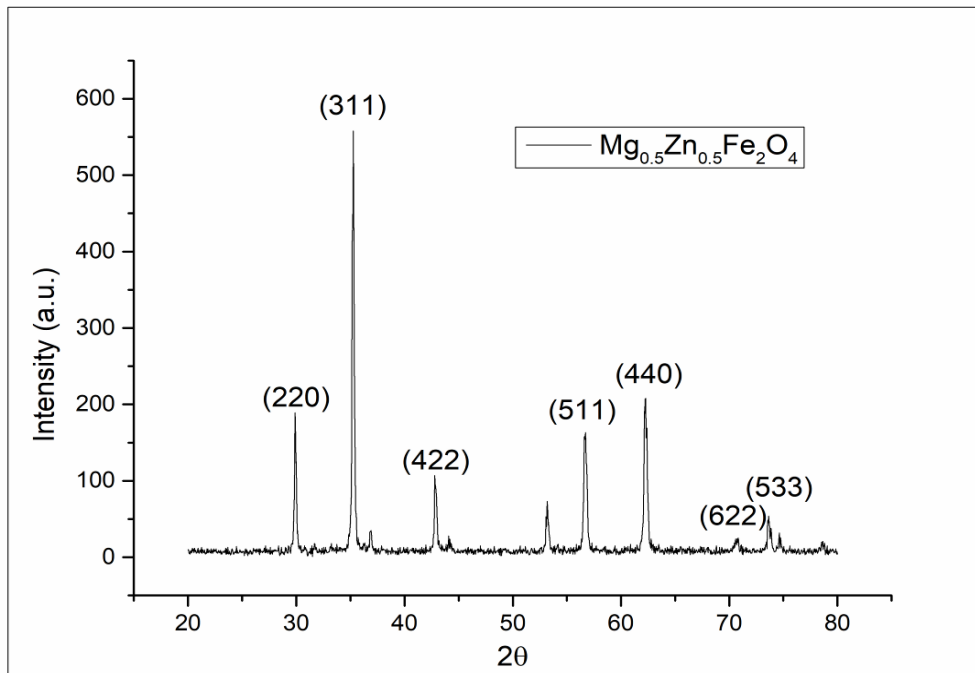


Figure 11: Indexed XRD pattern for $Mg_{0.5}Zn_{0.5}Fe_2O_4$

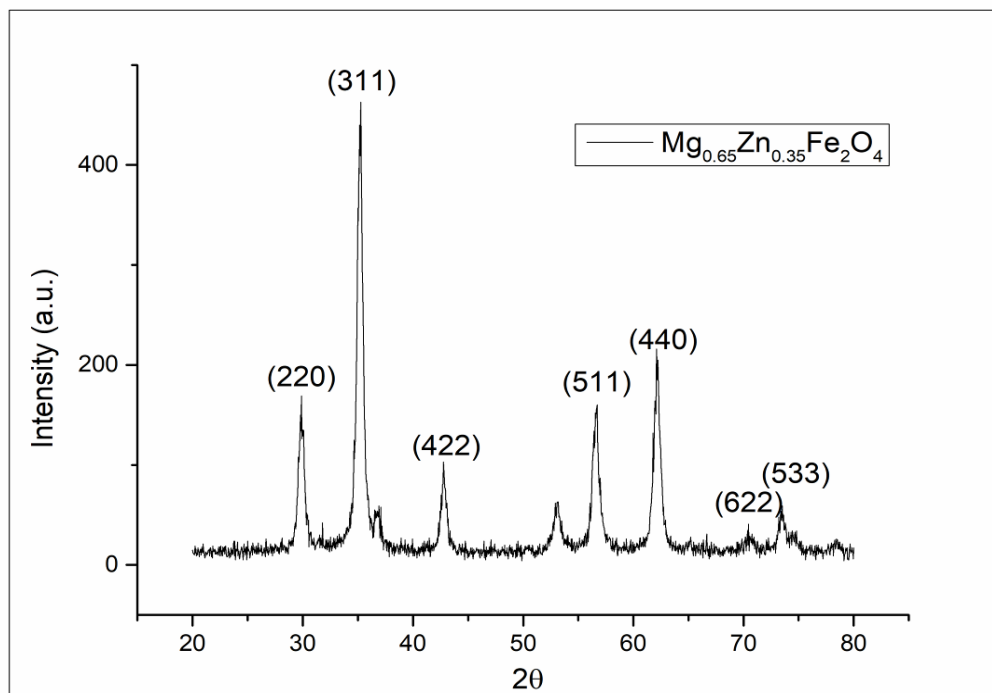


Figure 12: Indexed XRD pattern for $Mg_{0.65}Zn_{0.35}Fe_2O_4$

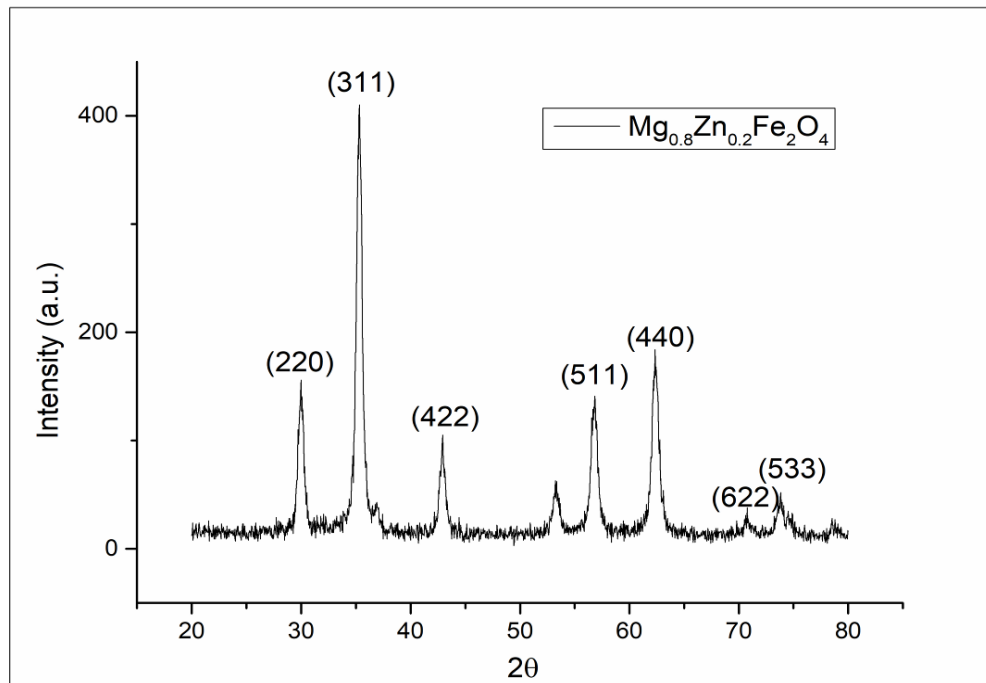


Figure 13: Indexed XRD pattern for $\text{Mg}_{0.8}\text{Zn}_{0.2}\text{Fe}_2\text{O}_4$

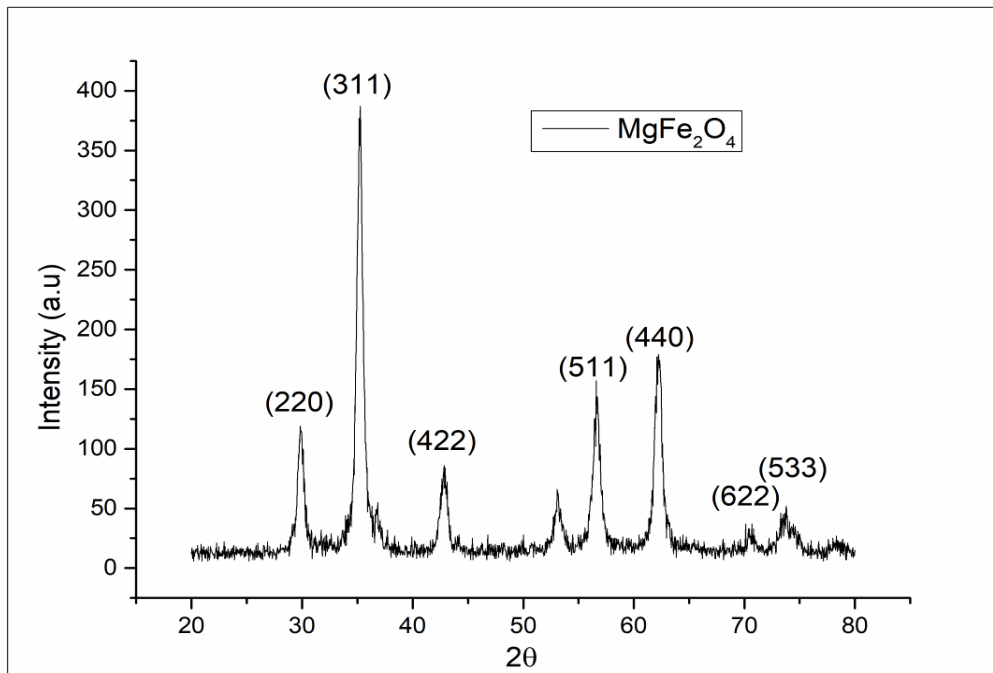


Figure 14: Indexed XRD pattern for MgFe_2O_4

Structure and morphology:

The X-ray patterns of our synthesized samples of $Mg_{1-x}Zn_xFe_2O_4$ (calcined at 800 °C for six hours) at room temperature are shown in Figures 8-14. XRD patterns indicate the formation of well distinct sharp peaks (111), (220), (311), (400), (422), (511), (440) and (533) for each sample, and in accordance with card number JCPD 01-089-1012 it confirmed the formation of FCC spinel phase. The purity of the prepared samples is clearly evident from the absence of other peaks in the diffractographs. The intensities of the planes (511), (440) and (220) are comparatively sensitive to the allocation of cations on tetrahedral and octahedral sites. There decreasing trend in the intensity of (440), (220) and (533). This shows settlement of Mg^{+2} ions on both octahedral and tetrahedral sites during Mg^{+2} doping process. The crystallite size calculated from Debye-Scherrer formula $t_{(311)} = K\lambda/\beta\cos\theta$ (where λ is the X-ray wavelength with a value of 1.5401 Å and K is the shape factor having a value of 0.9, θ is the Braggs angel and β is the FWHM) showed a decreasing trend with increasing Mg^{+2} concentration, which was also evident from peak broadening of the (311) (most intense peak) plane. This peak broadening and size reduction indicates that Mg atoms integration in the zinc ferrite spinel structure is homogenous. The composition vs crystallite size is shown in Table 5. With increase in Mg^{+2} ions concentration the decreasing trend in crystallite size can be explained by the replacement of Zn^{+2} ions, with larger ionic radii of 0.82 Å, by smaller Mg^{+2} ions (ionic radii 0.66 Å). There is an increase in porosity fraction ($P=1-(\rho_m/\rho_{xrd})$), (where ρ_{xrd} is the X-Ray density and ρ_m is the bulk density), owing to the decrease in cationic radii of substituted divalent metal ions as shown in Table-5. X-Ray density was observed to decrease linearly as shown in the Table 5 ($\rho_{xrd}=8M/Na^3$, where a is the lattice constant, N is the Avogadro's number and M is the molecular weight). This linear decrease can be accounted for the replacement of higher atomic weight Zn^{+2} ions with lower atomic weight Mg^{+2} ions. The unit cell volume also decreases with decrease in mass, thus the decrease in bulk density is evident as shown in the Table-5. As samples in powder forms are often porous in nature, $D_{Bulk} < D_{XRD}$ is well justified. The lattice constant a (calculated using the equation $a=d_{(hkl)}[h^2+k^2+l^2]^{1/2}$ where (h k l) are the miller indices and d is the inter planar spacing) also decreases with the increase in the substitution of Mg^{+2} ions (shown in Table 5). The various parameters obtained from XRD data are shown in Table 5.

Table 5: Crystallite size (nm), Lattice constant (Å), Volume of unit cell (Å)³, Bulk density(g/cm³), X-Ray density(g/cm³) , Porosity fraction(P)

Concentration	X=0.0	X=0.2	X=0.35	X=0.5	X=0.6	X=0.8	X=1.0
t(311) nm	34.2	29.4	27.6	26.8	23.4	21.1	19.2
a (Å)	2.5445	2.5432	2.5422	2.5418	2.5403	2.5398	2.5313
V(a ³)(E-22)	6.01	6.00	5.99	5.99	5.98	5.98	5.92
ρ_m (g/cm ³)	3.06	2.92	2.83	2.71	2.61	2.49	2.37
ρ_x (g/cm ³)	5.33	5.15	5.02	4.89	4.76	4.62	4.49
P(fraction)	0.426	0.433	0.437	0.446	0.452	0.461	0.471

The SEM images (shown in Figures 15-17) were used to determine the morphology of pure and magnesium substituted zinc ferrite nano-particles.

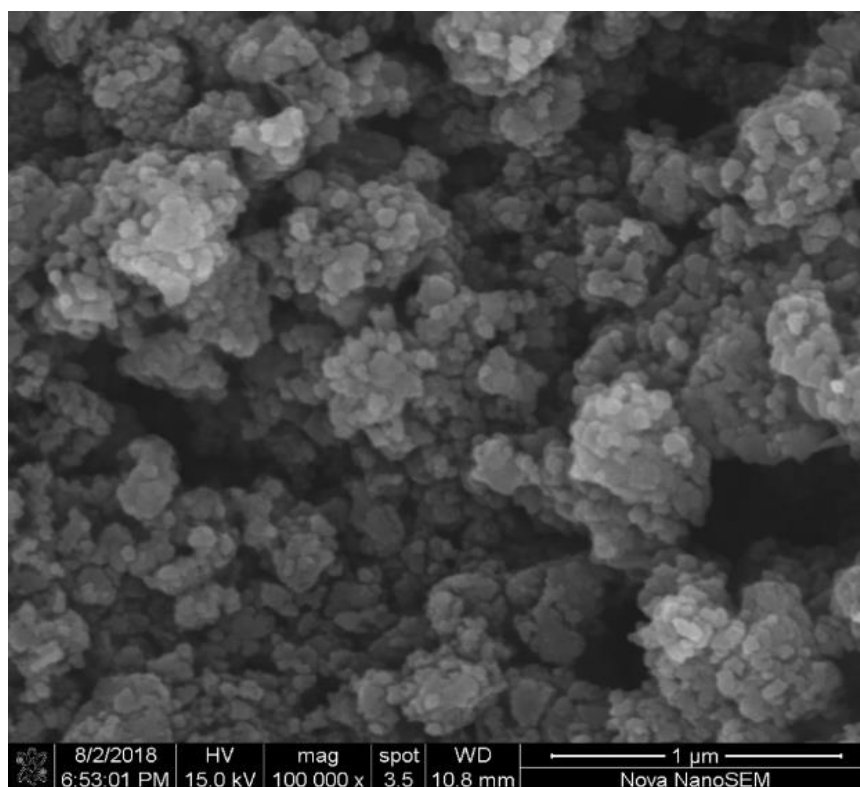


Figure 15: SEM image of ZnFe₂O₄

The SEM images showed nano-spherical formation of particles, however, agglomerates were also observed owing to the heat treatment (calcination) resulting in better diffusion of the atoms, causing the formation of agglomerates. The SEM images show no impurity phase confirming the efficiency of the chemical wet route (co-precipitation) method.

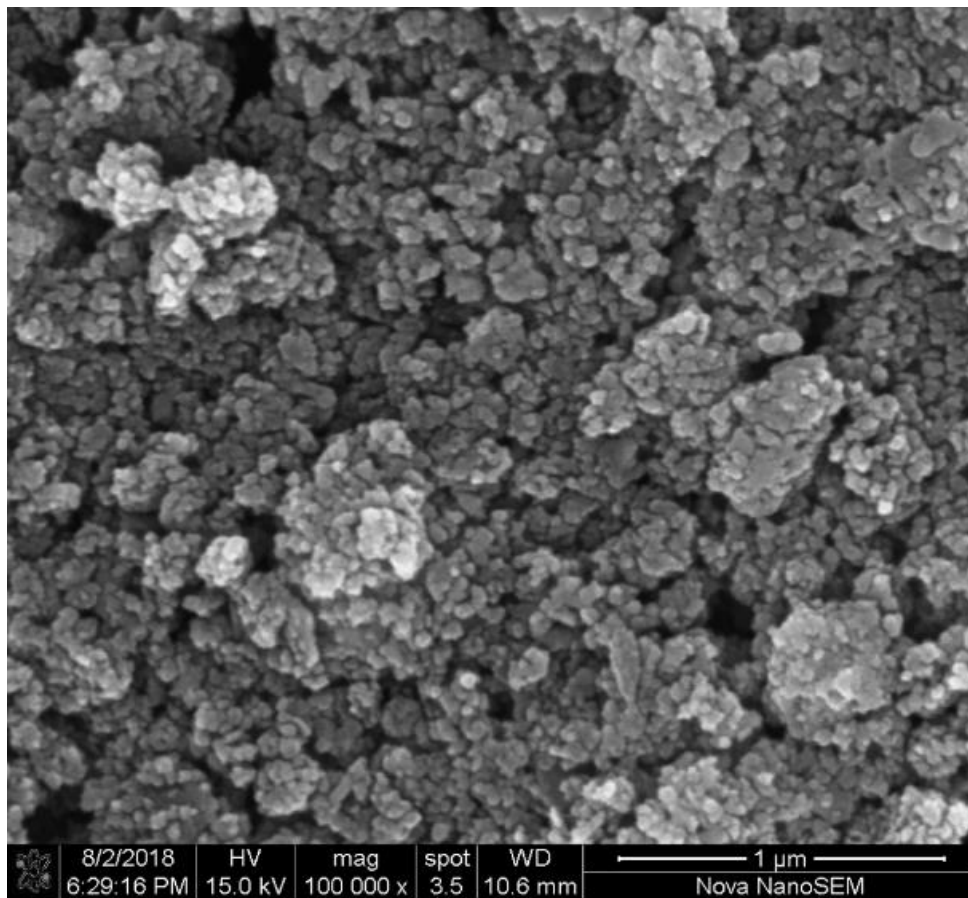


Figure 16: SEM image of $Mg_{0.5}Zn_{0.5}Fe_2O_4$

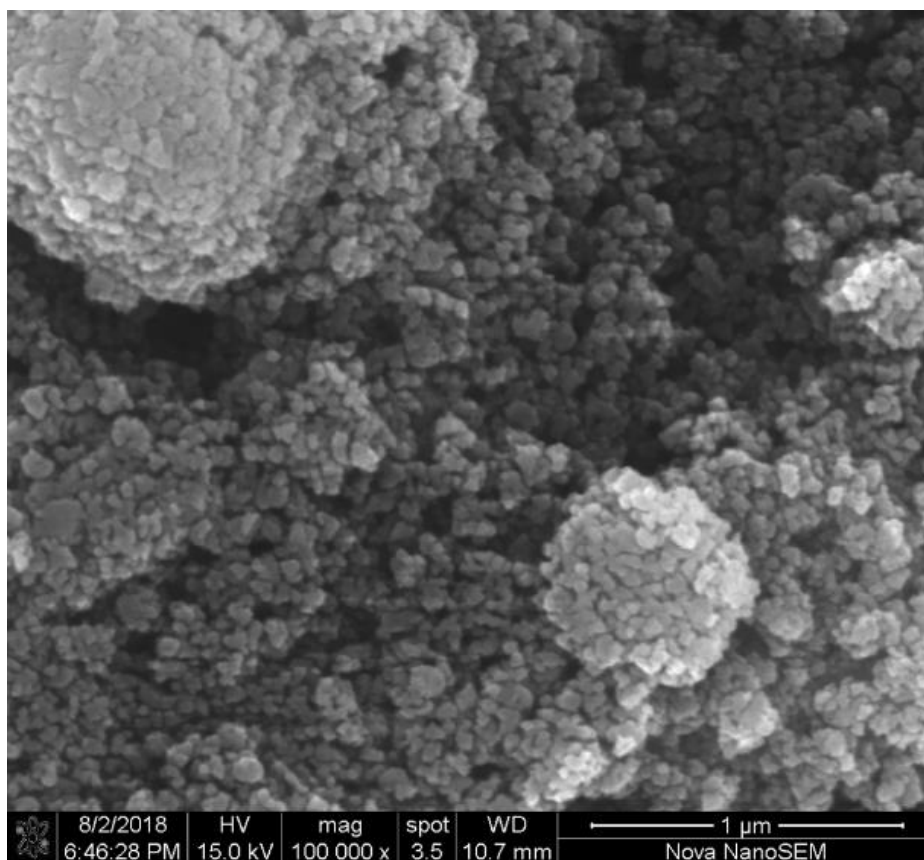


Figure 17: SEM image of MgFe₂O₄

FTIR Spectra:

The FTIR spectra is often utilized to investigate the structure of a multi-component system. The FTIR spectra of our synthesized samples was observed at room temperature, which supported the creation of spinel structure and its cationic distribution. As shown in Fig.18, two characteristic absorption bands were persistently found in the frequency range of 390 cm^{-1} to 600 cm^{-1} , which are also in agreement with those reported for the same ferrite family [1-3]. As metal ions in ferrites are situated at two different lattice positions, namely Tetrahedral (A) and Octahedral (B), stretching of these geometrical sites give rise to a band around 600 cm^{-1} for intrinsic tetrahedral metal complex (mutual bond formation among oxygen /tetrahedral site metal ions) around 400 cm^{-1} for intrinsic octahedral metal complex (mutual bond formation among oxygen /octahedral site metal ions).The presence of these lattice configurations verify the formation of spinel structure. It can also be observed that the bands are also shifting towards higher frequency region with increasing magnesium

substitution which can be explained by changes in bond length among the metal ions in their lattice positions. This shifting can also be explained on the basis of inverse relationship between force constant and reducing mass. Mg doping results in reduced mass on both A and B sites [19]. This increase in reduced mass decreases the force constant, causing the frequency shift as shown in Fig.18. The formation of spinel structure of ferrite samples is evident from the presence of these

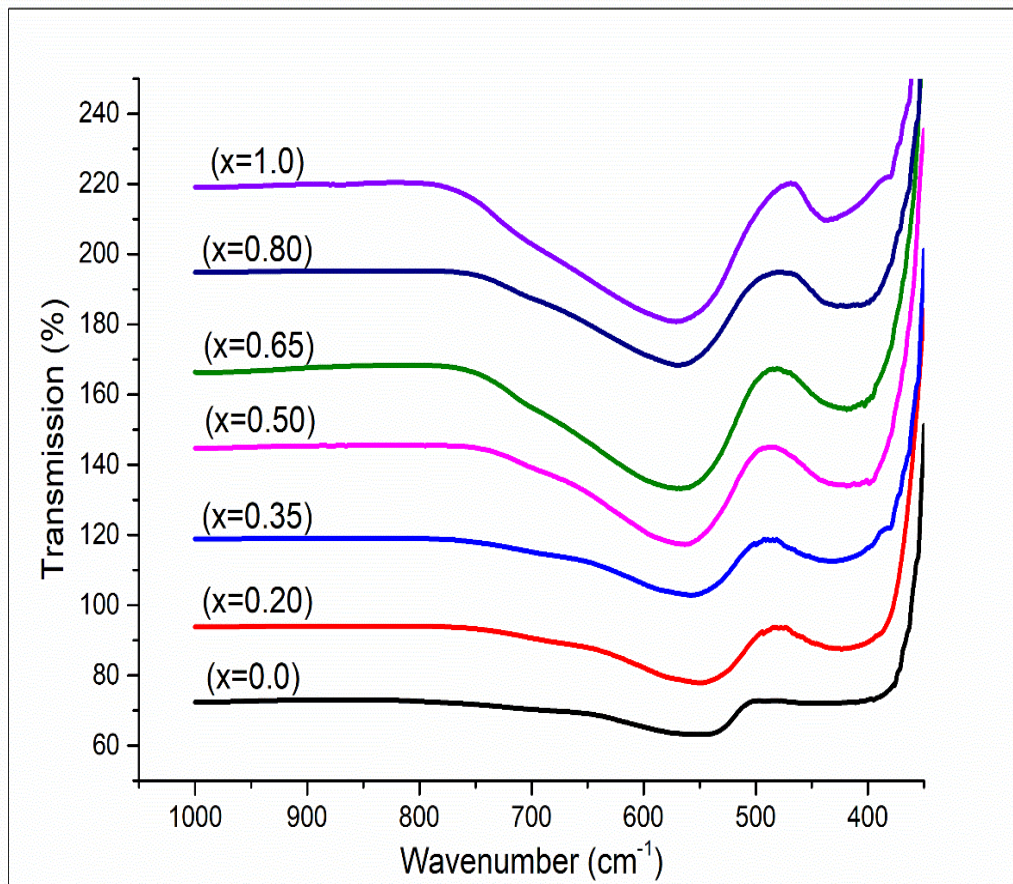


Figure 18: FTIR Spectra of synthesized ferrites

absorption bands.

Dielectric Measurements:

Dielectric properties of the synthesized samples were measured by making solid powder pellets (compressed to 5 tons with 10 mm dia) of the powdered samples. The variation of

dielectric constant ϵ' ($\epsilon' = Cd/A\epsilon_0$, where d is the thickness of the pellet, C is the capacitance, ϵ_0 is the permittivity of free space and A is the surface area of the pellet) against frequency (100Hz to 5MHz) for the synthesized compositions of $Zn_{1-x}Mg_xFe_2O_4$ measured at room temperature is shown in Fig.19, revealing dielectric dispersion as indicated by Maxwell-Wagner model of interfacial polarization, which is also in agreement with Koop's phenomenological theory.

A general frequency dependent behavior can be observed for all samples, showing a decreasing dielectric constant with increasing frequency. According to Maxwell Wagner model of inhomogeneous double layered solid structures, a dielectric solid is made up of two layers, well conducting grains and poor conducting grain boundaries. At low frequency, the electron hopping usually takes place due to $Fe^{+2}-Fe^{+3}$ ions located on octahedral sites [20]. This hopping produces local electrons displacement in the direction of applied electric field as the electrons get piled up at the resistive grain boundaries, thus producing space charge polarization ergo high dielectric values at low frequency. However, a finite time is required by space charge carriers to align their axis of arrangement with the applied alternating field. At higher frequencies, this electron exchange of $Fe^{+2}-Fe^{+3}$ lags behind in response to rapidly alternating external electric field due to the existence of lattice defects, oxygen vacancies or porosity etc., accounting for rapid decline in dielectric constant with increasing frequency. Figure 19 shows the variation of real dielectric constant (ϵ') and Figure 20 shows the imaginary dielectric constant (ϵ'') as a function of frequency for samples $Mg_xZn_{1-x}Fe_2O_4$ (where $x=0.0, 0.2, 0.35, 0.5, 0.65, 0.8, 1.0$) spinel ferrite in the frequency range from 5-120 kHz at room temperature.

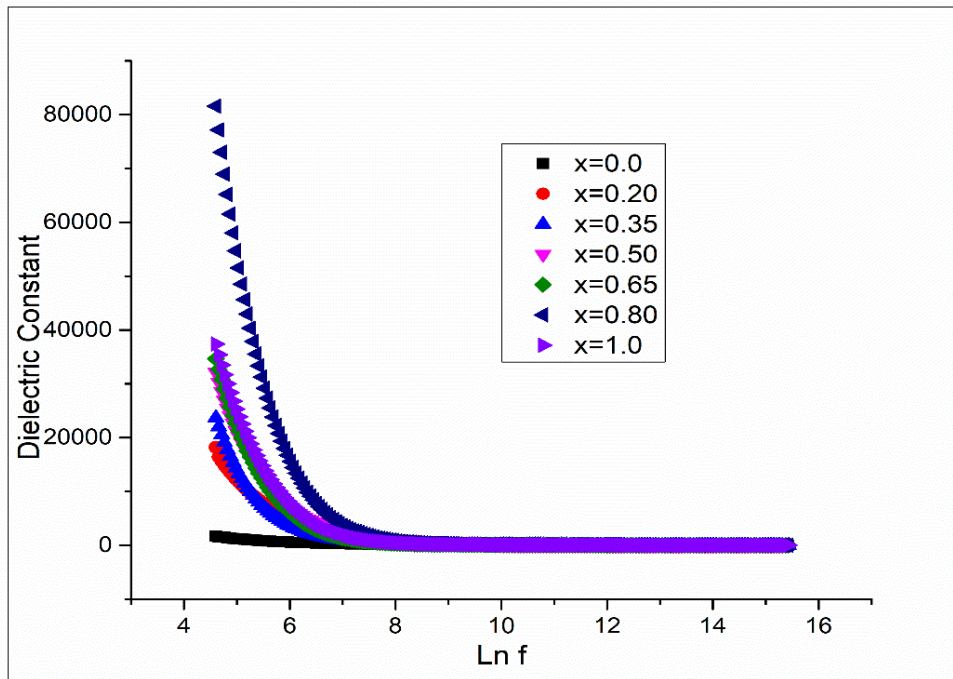


Figure 19: Dielectric Constant as a function of frequency

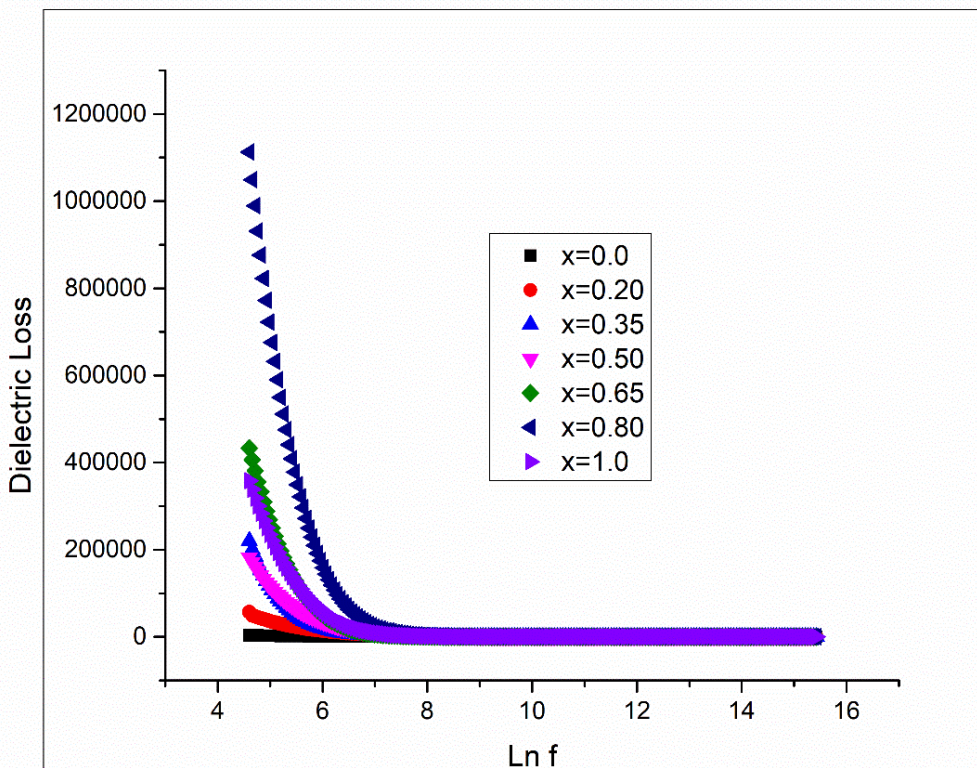


Figure 20: Dielectric Loss as a function of frequency

Dielectric constant ϵ' and dielectric loss factor ϵ'' account for energy dissipation and charge storage capacity/polarization ability. Dielectric constant ϵ' and dielectric loss ϵ'' show a high value at low frequencies for all samples however it starts to decrease at high frequency and finally becomes saturated. This type of behavior is normally observed in most of the ferrite composites. Dielectric constants of ferrites frequency dependent behavior, follow the Maxwell-Wagner's theory of interfacial polarization which is in accordance with Koop's theory. High values of dielectric constant at low frequencies are mainly caused by the predominance of Fe^{+2} ions, interfacial dislocation pile-ups, oxygen vacancies, different kind of polarizations (electronic, atomic, interfacial, and ionic etc.) and grain boundaries [21]. Due to the electronic exchange between the ferrous and ferric ions at high frequency the dielectric constant decreases. As the frequency continues to increase, the space charge polarization will start to move before reversing its direction and thus making no contribution virtually to the polarization and finally ϵ' becomes saturated.

The monotonous dispersion of dielectric values can be attributed to the substitution of increasing Mg^{+2} contents in the lattice structure. Mg^{+2} ions have the tendency to reside in both tetrahedral (A) and octahedral (B) sites, thus generating competition between Fe^{+2} and Fe^{+3} ions to occupy tetrahedral and octahedral sites. So as a growing number of Mg^{+2} ions occupy A-sites, some of the Fe-ions from B-Site will move to the A-site, resulting in the decline of the Fe^{+3} ions at octahedral sites, which are basically responsible for the conduction [22]. So the introduction of cationic ions has modified the dielectric constant of Mg substituted zinc ferrite. The highest dispersion value of dielectric constant for $x=0.80$ may appear due to the Fe^{+2} formation on octahedral sites, resulting in less resistive grain boundaries.

The dielectric loss ϵ'' also reveals the same intrinsic behavior of decreasing with increasing frequency until it becomes independent of frequency as shown in Fig.20 (calculated using the relation $\epsilon'' = \epsilon' \tan\delta$). The reason behind the surfacing of dielectric loss is the intrinsic lagging response of the dielectric material against the increasing frequency since as low frequency corresponds to high resistance (governed by grain boundaries), making the hopping mechanism at octahedral sites possible only at the expense of more energy, thus indicating high energy loss. During low frequency region, the dielectric loss is governed by

peak conductance. However, with increasing frequency, it decreases owing to the phenomenon of dielectric relaxation and leakage conductivity. The variation trend for dielectric loss tangent for the respective prepared compositions against the increasing frequency is shown in Fig.20.

Tan delta general increasing trend arises from inhibition or pinning of the domain wall motion. The shifting of peaks towards high frequency with increasing Mg^{+2} ions contents indicates that the hopping probability increases with increasing Mg^{+2} contents which can be attributed to more Fe^{+2} ions formation on octahedral sites. Furthermore, the small values of $\tan\delta$ verifies the presence of homogeneous structure rendering the use of this material for microwave applications.

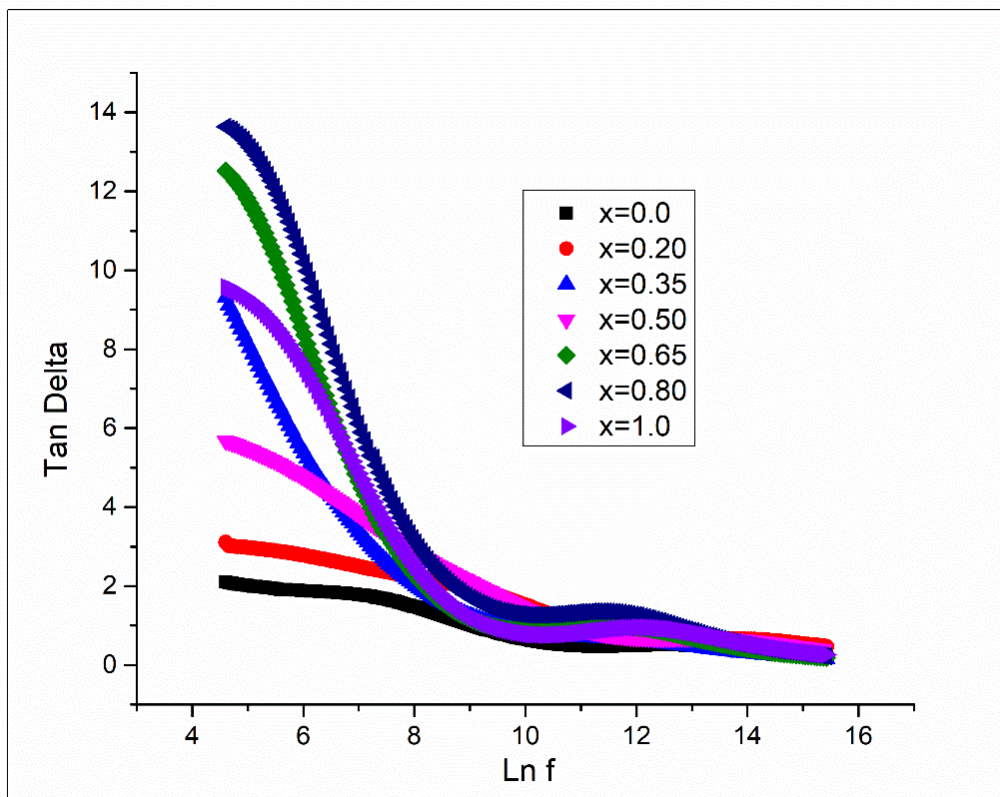


Figure 21: Tan Delta as a function of frequency

The deviation of AC conductivity ($\sigma_{AC}=2\pi f\epsilon_0\epsilon''$) against frequency measured at room temperature is shown in Fig.22. In order to understand the behavior, its figure can be divided into three different regimes namely regime 1: Low frequency Plateau, regime 2: Mid frequency plateau and regime 3: High frequency plateau.

The regime 1 can be explained on the basis of hopping between Fe^{+2} and Fe^{+3} ions at lower frequency. This region also corresponds to successful hopping of ions due to availability of prolonged time periods at low frequency. The regime 2 undergoes two types of mechanisms, successful hopping (the ion after hopping stays on the new site) and unsuccessful hopping (hopping ions jump back to their initial site). Both these relaxation processes compete during

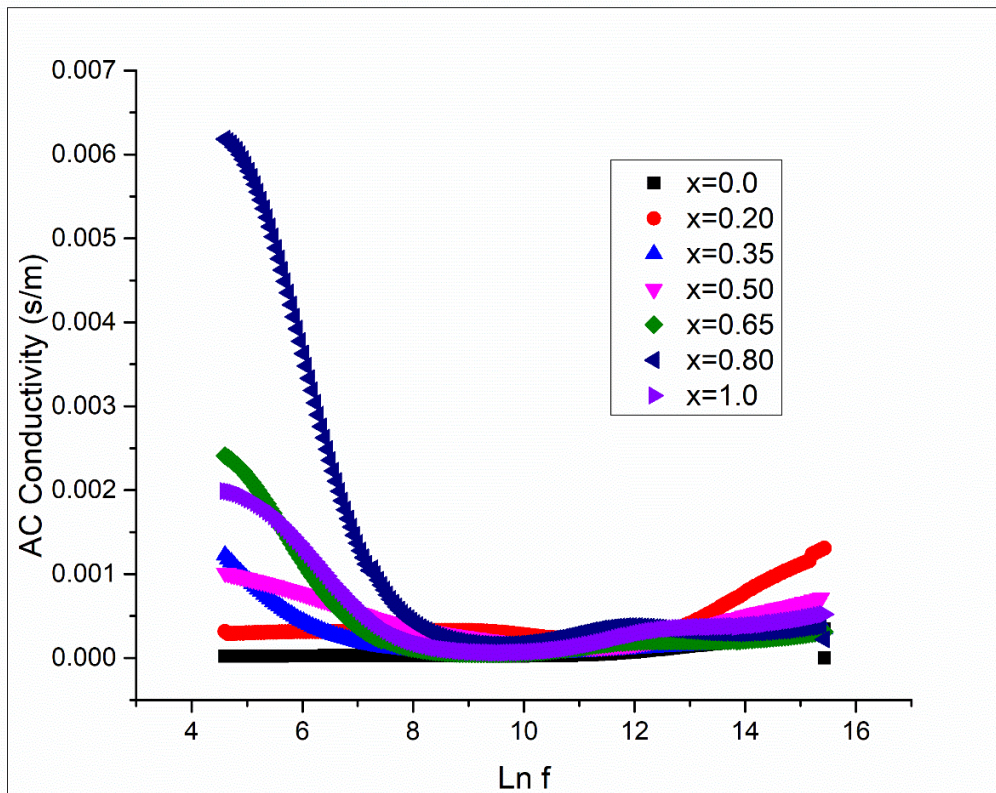


Figure 22: AC-Conductivity as a function of frequency

this frequency range and the increase or decrease in ratio of successful or unsuccessful jumping determines this dispersive regime i.e. the regime indicates the two competing

phenomenon namely, translational and reorientational mechanism. The regime 3 corresponds to the dominance of reorientational hopping (vibration about mean position) due to the lack of time period needed to successfully jump to distant lattice sites.

Complex Electric Modulus:

Complex electric formalism (an electric analogue to shear modulus) is an effective approach to study the frequency dependent dynamic response of conductive transport processes including carrier hopping rates, electrical charge relaxation time and space charge polarization, along with the dominance of minimal capacitance value present in the dielectric system, which results in an added advantage of electrode polarization effect suppression. As such, it can discriminate the grain boundary conduction from the electrode polarization while conveniently representing the electric field relaxation in the ceramic material when the dielectric displacement retains a constant magnitude. Fig.23 depicts the frequency dependent variation of real part M' of elastic modulus ($M' = \epsilon''^2 / \epsilon'^2 + \epsilon''^2$).

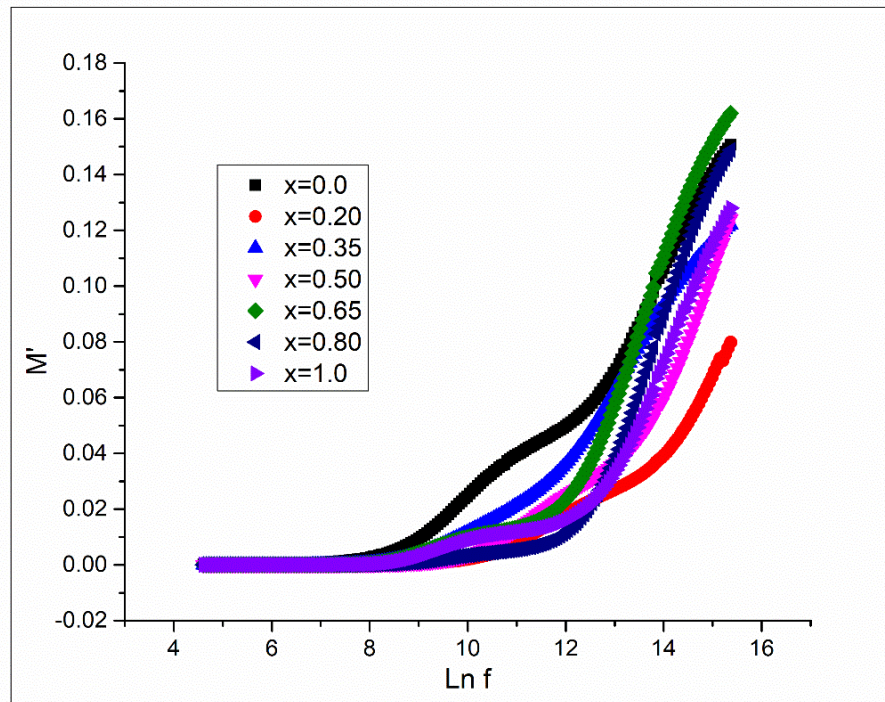


Figure 23: Variation of real (M') complex electric modulus as a function of frequency

The obtained spectra for various compositions is characterized by very small values (almost approaching to zero) during low frequency region which reveals the ease of polaron hopping. Such a behavior supports the long range mobility of charge carriers, supporting the electrode polarization. However, a continuous sigmoidal increase with increasing frequency was also observed, which eventually reaches to a maximum asymptotic value at highest frequency value. This increase with continuous dispersion on increasing frequency can be attributed to short range mobility of charge carriers due to the absence of restoring force under the influence of steadily induced electric field [23]. Fig. 24 shows the frequency dependent variation of imaginary component M'' of electric modulus ($M'' = \epsilon'' / \epsilon'^2 + \epsilon''^2$) exhibiting maxima at specific high frequency. It provides more refined information related to charge transport mechanism such as long to short order charge transport shifting or vice versa, charge relaxation time and dynamics of carrier ions as a function of frequency. The dispersed M'' Spectrum against frequency variation is characterized by a). well resolved peak formation at characteristic frequency range b). large asymmetry in peak formation and c). shifting of peaks from high frequency region towards low frequency region.

The formation of peak is governed by the region which indicates transitioning from long range to short range carrier mobility, providing a dispersion of conductivity relaxation time which is related to hopping probability which increases at low frequency. The large asymmetrical broadening of peaks is indicative of relaxation time dispersion with time constant variation. Such broadening is found to be increased with increasing substitution of magnesium, which in turn depicts the overlapping of potential wells (to which carriers are bound) between long and short range order. The origin of this dispersion is the increase in inhomogeneity of carriers by increasing substitution of magnesium. Hence, the conductivity relaxation is of non-Debye type.

The shifting of peaks towards lower frequency region is in correspondence with increase in relaxation time, indicating a correlation between the motions of different mobile ions. The overall pattern depicts the increasing possibility of long range order of carriers via hopping.

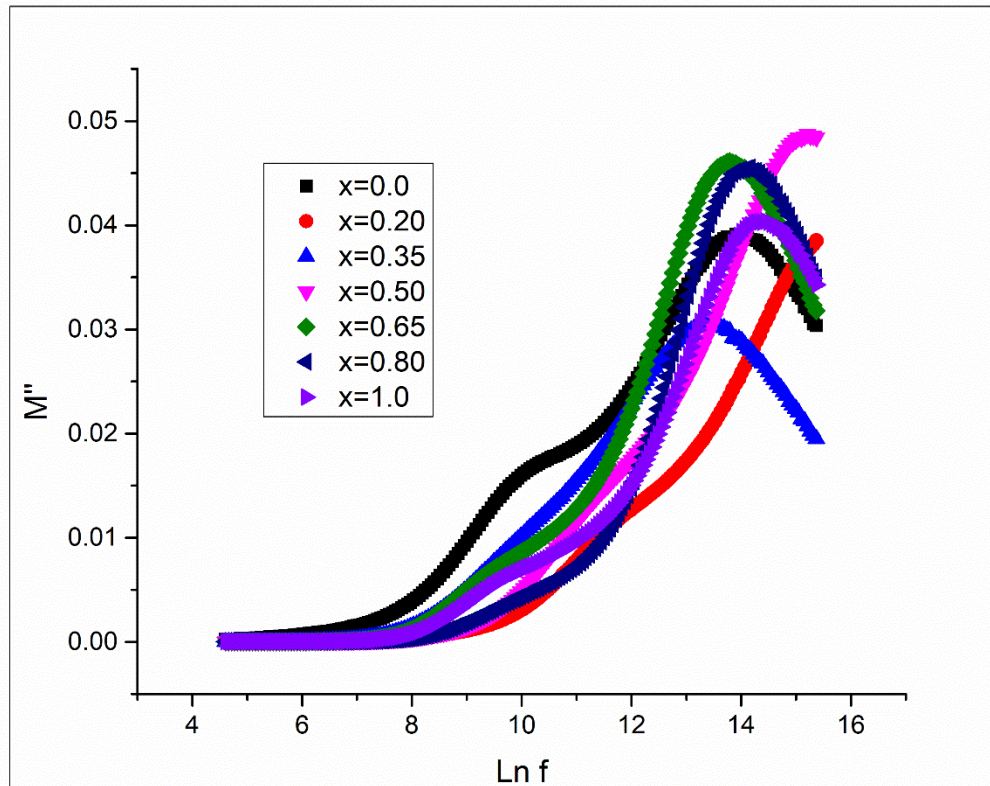


Figure 24: **Imaginary(M'') parts of complex electric modulus as a function of frequency**

The complex spectrum (Cole-Cole plot) using M'' and M' as variables is plotted in Fig. 25 for better understanding of the bulk structure where a large portion of volume is occupied by grain boundary region.

The typical characteristics of a Cole-Cole plot include i). effect of grains and grains boundary at higher and lower frequency, resulting in formation of deformed semicircles and ii). increase in radii of deformed semicircles with a gradual shift towards lower frequency region as Mg contents are increased. As described in XRD analysis, the overall size parameters of nano-ferrite are getting smaller with increasing substitution, therefore, an increase in grain boundary density is predictable. Such an effect is visible in contribution to conductivity via grain boundary density. The lower frequency region i.e. the extreme left of the semicircle represents grain resistance while the intermediate frequency region corresponds to grain boundary resistance [24]. The high frequency region on the extreme right corresponds to the whole resistance from both grain and grain boundary. The centers

of these deformed semicircles lie below the real axis, depicting the dispersion of relaxation time, thus confirming non-Debye type relaxation. The increasing radii of the semicircles can be accounted for the fact that the addition of Mg reduces the grain growth, resulting in high grain boundary density which leads to high grain boundary resistance.

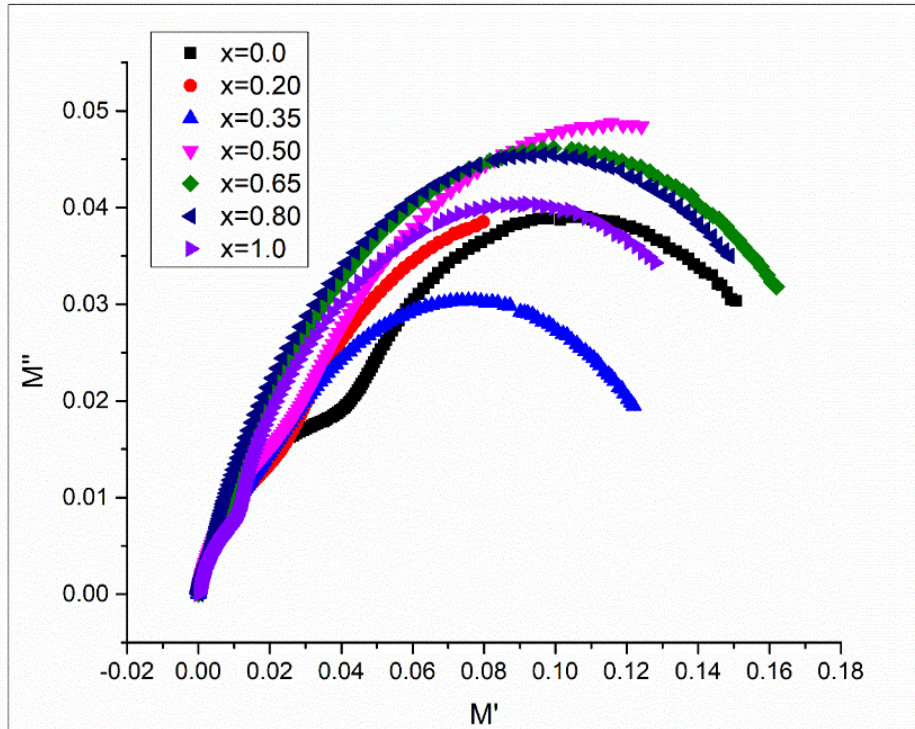


Figure 25: Cole Cole plot (M'' Vs M')

Conclusion:

In the present work, Zinc nanoferrite (ZnFe_2O_4) particles were synthesized using wet chemical route (co-precipitation). The X-ray powder diffraction technique was used to determine the phase formation. The obtained XRD pattern confirmed the formation of face centered cubic close pack arrangement of nanoparticles. No additional peaks were observed, confirming the purity of the substance. The crystallite size, calculated using the Scherer formula, was in the range of 19.2 nm to 34.2 nm showing the formation of small grains. The gradual decrease in crystallite size was found with increasing Mg^{+2} concentration, thereby reducing the grain size. The decrease in bulk density, X-Ray density as well as increase in porosity fraction was observed with addition of Mg^{+2} owing to small radii (0.66 Å) of substituted atom as compared to Zn^{+2} radii (0.82 Å). The SEM images confirmed the formation of nanoparticles. The agglomerates were also observed owing to the heat treatment (calcination) resulting in better diffusion of the atoms, causing the formation of agglomerates. The FTIR spectra showed configurational vibrations of both tetrahedral (A) and octahedral (B) sites, confirming the formation of spinel structure. Further, the tetrahedral and octahedral bands shift towards higher wavenumber with increase in Mg^{+2} ions. The particles sizes found in SEM images were in complete agreement with the results of XRD. The dielectric constant (ϵ') showed increased values dispersion at low frequency region and decreased values at high frequency which were found to be in agreement with Koops theory. The dielectric loss factor was found to increase massively which show their suitability to use for microwave applications. The AC conductivity showed mixed trend of magnesium and zinc ferrite nature, dominating each other. AC-conductivity (σ_{AC}) showed trend of variation with increasing frequency which was explained due to successful translational hopping and unsuccessful reorientational vibration. The high dielectric loss (ϵ'') values could be attributed to high energy losses. The minimal $\tan\delta$ values at high frequency indicated the synthesized ferrite to be a potential candidate for microwave applications. The experimental route proved to be an efficient, inexpensive and environmental friendly straight forward procedure for the synthesis of $\text{Mg}_{1-x}\text{Zn}_x\text{Fe}_2\text{O}_4$ nanoparticles, without harmful byproducts, which can also be used for the synthesis of other spinel ferrite substitutions.

Future Work:

Magnesium-Zinc ferrites can absorb electromagnetic spectrum, so the studies of their microwave absorption as well as UV-Vis characterization can relate to important data which can be deployed for military applications. Often, to make the polymer blends somewhat conductive, different metallic media are added using various polymerization techniques. It's only natural that the next step regarding this research would be to add such a nanohybrid in a polymer matrix to study the mechanical as well as microwave properties of Mg-Zn ferrite nanoparticles. Owing to their enhanced dielectric properties, such a can be used in batteries cathode as well as in the construction of aerospace parts by incorporation of thermoset resins rendering them high stiffness and strength even at very high temperatures. With the advancement in the field of composites and their versatile use in various industries, such a composite can revolutionize the field of nanoscience's as well as nanotechnology, pushing the boundaries in the realm of magnetism, dielectric, optical and electromagnetic application.

References

- [1] Mathew, D.S. and R.-S. Juang, An overview of the structure and magnetism of spinel ferrite nanoparticles and their synthesis in microemulsions. *Chemical Engineering Journal*, 2007. **129**(1-3): p. 51-65.
- [2] Rahman, O.u., S.C. Mohapatra, and S. Ahmad, Fe₃O₄ inverse spinel super paramagnetic nanoparticles. *Materials Chemistry and Physics*, 2012. **132**(1): p. 196-202.
- [3] Ederer, C. and N.A. Spaldin, Weak ferromagnetism and magnetoelectric coupling in bismuth ferrite. *Physical Review B*, 2005. **71**(6).
- [4] Morin, F.J., Oxides Which Show a Metal-to-Insulator Transition at the Neel Temperature. *Physical Review Letters*, 1959. **3**(1): p. 34-36.
- [5] Bedanta, S. and W. Kleemann, Supermagnetism. *Journal of Physics D: Applied Physics*, 2009. **42**(1): p. 013001.
- [6] Hong, X., et al., A novel ternary hybrid electromagnetic wave-absorbing composite based on BaFe_{11.92}(LaNd)_{0.04}O₁₉-titanium dioxide/multiwalled carbon nanotubes/polythiophene. *Composites Science and Technology*, 2015. **117**: p. 215-224.
- [7] A.Pradeep, P.Priyadharsini and G.Chandrasekaran., Structural, magnetic and electrical properties of nanocrystalline zinc ferrite. *Journal of Alloys and compounds*. 2011. 509(9):p.3917-3913
- [8] Li, J., et al., Bottom-up versus top-down effects on ciliate community composition in four eutrophic lakes (China). *European Journal of Protistology*, 2016. **53**: p. 20-30.
- [9] Simon, P. and Y. Gogotsi, Materials for electrochemical capacitors. *Nat Mater*, 2008. **7**(11): p. 845-854.
- [10] Yoon, T.J., et al., Multifunctional nanoparticles possessing a "magnetic motor effect" for drug or gene delivery. *Angew Chem Int Ed Engl*, 2005. **44**(7): p. 1068-71.
- [11]. Hung, K., et al., Wide-temperature range operation supercapacitors from nanostructured activated carbon fabric. *Journal of Power Sources*, 2009. **193**(2): p. 944-949.

- [12] Yu, G., et al., Hybrid nanostructured materials for high-performance electrochemical capacitors. *Nano Energy*, 2013. **2**(2): p. 213-234.
- [13] Gul, I.H., et al., Structural, magnetic and electrical properties of $\text{Co}_{1-x}\text{Zn}_x\text{Fe}_2\text{O}_4$ synthesized by co-precipitation method. *Journal of Magnetism and Magnetic Materials*, 2007. **311**(2): p. 494-499.
- [14] Zhang, Y., et al., Composition and magnetic properties of cobalt ferrite nanoparticles prepared by the co-precipitation method. *Journal of Magnetism and Magnetic Materials*, 2010. **322**(21): p. 3470-3475.
- [15] Xie, H., et al., An improved continuous co-precipitation method to synthesize $\text{LiNi}_{0.80}\text{Co}_{0.15}\text{Al}_{0.05}\text{O}_2$ cathode material. *Journal of Alloys and Compounds*, 2016. **666**: p. 84-87.
- [16] Melo, R.S., et al., Magnetic ferrites synthesised using the microwave-hydrothermal method. *Journal of Magnetism and Magnetic Materials*, 2015. **381**: p. 109-115.
- [17] Güven Özdemir, Z., et al., Super-capacitive behavior of carbon nano tube doped 11-(4-cyanobiphenyl-4-oxy) undecan-1-ol. *Journal of Molecular Liquids*, 2015. **211**: p. 442-447.
- [18] Ali, A.A., et al., MWCNTs/carbon nano fibril composite papers for fuel cell and super capacitor applications. *Journal of Electrostatics*, 2015. **73**: p. 12-18.
- [19] Waldron, R.D., Infrared Spectra of Ferrites. *Physical Review*, 1955. **99**(6): p. 1727-1735.
- [20] Mirzaee, S., S.F. Shayesteh, and S. Mahdaviifar, Synthesis and Characterization of Cubic Omega-3-coated Cobalt Ferrite Nanoparticles. *Journal of Superconductivity and Novel Magnetism*, 2014. **27**(7): p. 1781-1785.
- [21] Szczygieł, I. and K. Winiarska, Synthesis and characterization of manganese–zinc ferrite obtained by thermal decomposition from organic precursors. *Journal of Thermal Analysis and Calorimetry*, 2013. **115**(1): p. 471-477.
- [22] Nikumbh, A.K., et al., Structural, electrical, magnetic and dielectric properties of rare-earth substituted cobalt ferrites nanoparticles synthesized by the co-precipitation method. *Journal of Magnetism and Magnetic Materials*, 2014. **355**: p. 201-209.

- [23] Dar, M.A., et al., Low dielectric loss of Mg doped Ni–Cu–Zn nano-ferrites for power applications. *Applied Surface Science*, 2012. **258**(14): p. 5342-5347.
- [24] Druc, A.C., et al., How cobalt ions substitution changes the structure and dielectric properties of magnesium ferrite? *Ceramics International*, 2014. **40**(8): p. 13573-13578.